


RESEARCH ARTICLE

Integrative Research on the Functional Logic of Neural Circuits

Temporal dynamics of neocortical development in organotypic mouse brain cultures: a comprehensive analysis

 Aniella Bak,¹  Katharina Schmied,¹  Morten L. Jakob,²  Francesco Bedogni,³  Olivia A. Squire,³  Birgit Gittel,¹  Maik Jesinghausen,²  Kerstin D. Schünemann,¹  Yvonne Weber,¹  Björn Kampa,^{2,4}  Karen M. J. van Loo,^{1,5} and  Henner Koch¹

¹Department of Epileptology, Neurology, RWTH Aachen University Hospital Aachen, Aachen, Germany; ²Systems Neurophysiology, Institute of Zoology, RWTH Aachen University, Aachen, Germany; ³School of Medicine, Neuroscience and Mental Health Research Institute, Cardiff University, Cardiff, United Kingdom; ⁴JARA BRAIN, Institute of Neuroscience and Medicine (INM-10), Forschungszentrum Jülich, Jülich, Germany; and ⁵Department of Neurosurgery, RWTH Aachen University Hospital Aachen, Aachen, Germany

Abstract

Murine organotypic brain slice cultures have been widely used in neuroscientific research and are offering the opportunity to study neuronal function under normal and disease conditions. Despite the broad application, the mechanisms governing the maturation of immature cortical circuits *in vitro* are not well understood. In this study, we present a detailed investigation into the development of the neocortex *in vitro*. Using a holistic approach, we studied organotypic whole hemisphere brain slice cultures from postnatal mice and tracked the development of the somatosensory area over a 5-wk period. Our analysis revealed the maturation of passive and active intrinsic properties of pyramidal cells together with their morphology, closely resembling *in vivo* development. Detailed multielectrode array (MEA) electrophysiological assessments and RNA expression profiling demonstrated stable network properties by 2 wk in culture, followed by the transition of spontaneous activity toward more complex patterns including high-frequency oscillations. However, culturing weeks 4 and 5 exhibited increased variability and initial signs of neuronal loss, highlighting the importance of considering developmental stages in experimental design. This comprehensive characterization is vital for understanding the temporal dynamics of the neocortical development *in vitro*, with implications for neuroscientific research methodologies, particularly in the investigation of diseases such as epilepsy and other neurodevelopmental disorders.

NEW & NOTEWORTHY The development of the mouse neocortex *in vitro* mimics the *in vivo* development. Mouse brain cultures can serve as a model system for cortical development for the first 2 wk *in vitro* and as a model system for the adult cortex from 2 to 4 wk *in vitro*. Mouse organotypic brain slice cultures develop high-frequency network oscillations at γ frequency after 2 wk *in vitro*. Mouse brain cultures exhibit increased heterogeneity and variability after 4 wk in culture.

electrophysiology; in vitro development; neocortical development; neuronal morphology; organotypic mouse brain slice cultures

INTRODUCTION

Due to the limitations of experimental animal models, which are costs, labor, and ethical concerns on animal numbers and suffering, many advances have been made during recent years to improve *in vitro* neurological models to better mimic the *in vivo* situation. Although induced pluripotent stem cells (iPSCs) and organoids have been a big step in the right direction and provide the advantage of recapitulating

human development in simplified neural networks (1), partially preserving genetic patient characteristics (2) and eliminating the ethical concerns tied to the use of embryonic stem cells (3), they unfortunately still encounter the problem of impaired maturation and lack of cellular diversity and structural complexity (4, 5). Although acute brain slices are a viable option to investigate the rodent brain at different ages relatively close to the *in vivo* situation, they, unfortunately, do not enable genetic modification, long-term stimulation, or



Correspondence: A. Bak (Aniella.va.bak@gmail.com); H. Koch (hkoch@ukaachen.de).
Submitted 24 April 2024 / Revised 5 August 2024 / Accepted 6 August 2024



pharmacological manipulation. Although these methods can be applied in living animals, *in vitro* preparations offer more precisely controlled experimental conditions. Organotypic brain slice cultures (oBSCs) close this gap by providing an experimental time frame of multiple weeks along with intact three-dimensional cytoarchitecture and the inclusion of all cellular subtypes of the brain. oBSCs have been widely adapted in neuroscientific research since they were first established by Gähwiler (6) with the initial roller tube culturing technique. Though this method is robust and yields stable cultures for multiple weeks (7–11), the thinning to 2–3 cell layers and therefore loss of the original spatial organization might be preferable for applications where visual accessibility is favored, but not for electrophysiological, morphological, and developmental studies that require the intact three-dimensional architecture of certain brain areas. As a consequence, the method was further adapted by Stoppini et al. (12), introducing a semiporous membrane culturing method at an air-liquid interface to preserve the original structure of brain preparations. Both methods have been shown to maintain the organotypic structure, their normal cell morphology and to generally correlate well with development observed *in vivo* (7, 9, 13–17), and have been used successfully in the past, investigating, for example, neurodegeneration (18, 19), ischemia (20–23), interneuron development (7, 10), axon formation and dynamics (24, 25), and network dynamics (15, 26, 27). In addition, oBSCs have been used as a screening platform for novel therapy targets and therapeutics (14).

Especially, preparations of the rat and mouse hippocampus have been used and characterized widely (11, 28–33) with only a limited number of studies reporting the use of other brain areas such as the cerebellum (13, 15, 34, 35), striatum (10, 36), or cortex (7, 9, 16, 37–39). Neocortical oBSCs are of special interest when it comes to the investigation of inhibition and excitation balancing, developmental network dynamics, cell-cell relationships, and pathogenesis in the maturing cortex. Unfortunately, to date, information on the tissue development *ex vivo* is scarce and has only been reported in cultures created by the initial roller tube technique (7–10, 25, 40–42) or in studies only focusing on specific parameters (24, 37–39, 43). This study aimed to close this gap of knowledge by providing a holistic characterization of the development of membrane insert-cultured mouse neocortical oBSCs over a time course of 5 wk, investigating single cell and network electrophysiology, RNA expression levels, and morphology of pyramidal cortical neurons, as this information will hold vital indications on which timeframes of culturing are suitable for different types of experimental approaches.

MATERIALS AND METHODS

Animals

All procedures involving animals were approved and performed in accordance with the guidelines of the Federation of European Laboratory Animal Science Association, the EU Directive 2010/63/EU, and the German animal welfare law. For harvesting of brain tissue for organotypic cultures, wild-type C57BL/6J mice (RRID: MGI:3028467) of either sex aged 5–7 postnatal days were used. Mice were obtained from the local Institute of Laboratory Animal Science RWTH University

Clinic Aachen and housed at a 12-h light-dark cycle with food and water *ad libitum*. Tissue harvest was performed after the decapitation of mice and both male and female animals were used. Experimental subjects were not randomized because this was deemed irrelevant to this study.

Slice Preparation

The slice preparation was performed on the bench but in sanitized conditions. After mouse decapitation without anesthesia, the brain was carefully extracted from the skull using microdissection tools. Hemispheres were separated and glued on solidified agarose blocks with the rostral side facing upward. Brain tissue was sliced perpendicular to the cortical surface at 350 μm and coronal whole hemisphere slices were used for cultivation. Brain slices were generated using a vibratome (Leica VT1200S, RRID: SCR_018453) filled with ice-cold artificial cerebrospinal fluid (aCSF), containing: 125 mM NaCl, 25 mM NaHCO_3 , 2.5 mM KCl, 1.25 NaH_2PO_4 , 1 mM $\text{MgCl}_2 \cdot 6\text{H}_2\text{O}$, 2 mM CaCl_2 , 25 mM glucose, and 1% penicillin/streptomycin (Gibco) dissolved in Millipore water. aCSF was constantly perfused with carbogen gas (95% O_2 and 5% CO_2) and kept cold by reusable plastic ice cubes for appropriate hypothermia and oxygenation during preparation. For all experiments, if not stated otherwise, somatosensory cortical regions of whole mouse brain slices were used and analyzed.

Organotypic Brain Slice Cultures

Under a sterile hood, slices were placed on semipermeable membrane inserts (pore size 0.4 μm , Millipore), adhered by removing excess liquid, and placed in 6-well plates at an air-liquid interface on 1.2 mL of controlled medium containing 20% horse serum (Invitrogen), 1 mM L-glutamine (Gibco), 0.00125% ascorbic acid (Sigma), 0.001 mg/mL insulin (Invitrogen), 1 mM CaCl_2 (Sigma), 2 mM MgSO_4 (Sigma), 13 mM glucose (Sigma), and 1% penicillin/streptomycin (Invitrogen) in minimum essential medium (MEM, Gibco) at an osmolarity of 320 mosmol/L and pH of 7.28. Cultures were exclusively handled in aseptic conditions as long as they were cultured and were maintained in an incubator with a controlled atmosphere (37°C, 5% CO_2 , 100% humidity) and full medium change was performed every two days.

Time Periods

All experiments on organotypic brain slice cultures were performed in a time frame of 1–37 days *in vitro*. For patch-clamp experiments, periods are defined as initial (1–2 days *in vitro*, DIV), *week 1* (6–9 DIV), *week 2* (11–16 DIV), *week 3* (17–23 DIV), *week 4* (28–30 DIV), and *week 5* (34–37 DIV). The remaining experiments were performed on the exact corresponding day, meaning initial (2 DIV), *week 1* (7 DIV), *week 2* (14 DIV), *week 3* (21 DIV), *week 4* (28 DIV), and *week 5* (35 DIV), ± 1 DIV. Experimenters were not blinded to the six time points as experiments were performed continuously over the time period of 5 wk, and the simultaneous maintenance of multiple cultures of different ages was not feasible.

Patch-Clamp Recordings

Whole-cell patch-clamp recordings on mouse organotypic brain slice cultures were performed at various time points

with cultures being in vitro between 2 and 37 days. For whole-cell patch-clamp recordings, slices were excised from the cultivation membrane by cutting the membrane around the slice with a scalpel and transferred to the recording bath. During recordings, slices were continuously perfused with carbogenated aCSF at 30°C at a perfusion rate of ~7 mL/min. Recording pipettes were pulled from borosilicate glass capillaries (World Precision Instruments) with a resistance of 3–7 MΩ. For recordings, pipettes were filled with intracellular solution containing: 140 mM K-gluconic acid, 1 mM CaCl₂, 10 mM EGTA, 2 mM MgCl₂, 4 mM Na₂ATP, 10 mM HEPES, and 5 mg/mL biocytin (Sigma). Neurons were patched within the somatosensory cortical region of whole mouse brain slices, approximately between 100 and 500 μm from the cortical border. Pyramidal cells were identified by their somatic shape and firing properties. Whole-cell recordings were performed using an EPC10 amplifier (HEKA, RRID: SCR_018399) and Patchmaster software (HEKA, RRID: SCR_000034). Signals were sampled at 10 kHz, filtered at 1 kHz, and analyzed using Fitmaster software (HEKA, RRID: SCR_016233) and custom-written MatLab (MathWorks, RRID: SCR_001622) scripts. After recordings, slices were fixed in 4% PFA (Morphisto) for 10–24 h.

Multielectrode Array Recordings

Multielectrode array (MEA) recordings on mouse organotypic brain slice cultures were performed at time points 2 DIV, 7 DIV, 14 DIV, 21 DIV, 28 DIV, and 35 DIV. Brain slices were excised from the cultivation membrane and transferred onto the MEA chip (256MEA30/8iR-ITO-pr, 16×16 electrodes, electrode size 30 μm, 200 μm spacing, Multi Channel Systems MCS GmbH) with the electrode grid covering most of the slice, especially the somatosensory cortical region. Slices were weighed down by a meshed harp and continuously perfused with carbogenated aCSF at a temperature of 30°C. Recordings were performed using a 256-electrode MEA system (USB-MEA 256, Multi Channel Systems MCS GmbH) with an electrode size of 30 μm and in-between electrode spacing of 200 μm. Signals were sampled at 10 kHz using Multi Channel Experimenter software (Multi Channel Systems MCS GmbH). After an equilibration period of 20 min, two consecutive recordings of 5 min were obtained and recordings were analyzed using custom scripts in MatLab (MathWorks, RRID: SCR_001622).

Immunohistochemistry

Free-floating organotypic slices were washed in PBS-T (0.1% Tween, Invitrogen; PBS 1×) for 10 min and then incubated in 0.1 M glycine in PBS for 30 min. Slices were washed in PBS-T (3 times, 15 min each) and incubated in blocking solution (10% horse serum, 1% triton in PBS) for 1 h, after which sections were incubated at 4°C with NeuN (1:500; Millipore, ABN78, RRID: AB_10807945) and parvalbumin (1:1,000; Sigma, P3088, RRID: AB_477329) or Tle4 (1:1,000; Santa Cruz, sc-365406, RRID: AB_10841582) and Ctip2 (1:500, Abcam, ab18465, RRID: AB_2064130) antibodies for 48 h. Following this, slices were thoroughly washed in PBS-T (10 times, 15 min each), and then incubated in the secondary antibody mix, consisting of AlexaFluor secondary antibodies (1:500, Thermo Fisher) and DAPI (1:500) in blocking solution, for 1 h at room

temperature. Slices were then washed twice in PBS-T, and mounted on slides with Fluoromount (Invitrogen). Images were acquired using either a Leica Upright Microscope or Zeiss LSM710 laser scanning confocal microscope.

RNA Isolation and cDNA Generation

For RNA isolation, two whole hemisphere slices from the same culturing insert were collected into one tube to obtain sufficient amounts of RNA. Tissue was homogenized by the addition of one 7-mm metal bead (steel, Qiagen) and 1 mL trizole (Invitrogen) per tube and inserting them into a SpeedMill (Analytik Jena) for 2 min. Subsequently, samples were centrifuged for 1 min at 1,000 rpm and 4°C, left on ice for 30 min, homogenized, and then left at room temperature for 5 min. Chloroform/trichloromethane (200 μL; Sigma) was added to each tube, vortexed for 60 s, and left at room temperature for 3 min. Samples were then centrifuged at 12.0 g and 4°C for 30 min and the aqueous phase was pipetted into new tubes. Isopropanol (400 μL) was added to each tube, mixed, and left at room temperature for 10 min. Subsequently, samples were centrifuged for 10 min at 12.0 g and 4°C, the supernatant was discarded and 800 μL of 75% ethanol was added. This step was repeated for a second time, then tubes were left upside down on a clean tissue to dry at room temperature. The pellet was finally taken up in 25 μL of nuclease-free water each and the amount of RNA was measured on a NanoDrop.

All samples showing sufficient RNA concentration (>100 ng/μL) and purity (260/280 ratio of 2.0 ± 0.2) were then used to generate cDNA by normalizing the sample with the lowest concentration to 15 μL volume and calculating the amount of RNA for remaining samples accordingly. To each sample of RNA, 4 μL of iScript reaction mix (Bio-Rad), 1 μL of iScript reverse transcriptase (Bio-Rad), and nuclease-free water to fill the total volume to 20 μL were added. cDNA was finally generated in a Thermocycler (Biometa) by priming at 25°C for 5 min, reverse transcription at 46°C for 20 min, and reverse transcriptase inactivation step at 95°C for 1 min.

RT-PCR

mRNA quantification was performed by real-time RT-PCR using the ΔΔCt-method. Quantitative PCR was performed in an QuantStudio I apparatus (Applied Biosystems, RRID: SCR_023003) containing 1× iQ SYBR Green supermix (Bio-Rad Laboratories Inc.), 5 pm of each oligonucleotide primer (*Actb*: 5'-CATTGCTGACAGGATGCAGAAGG-3' and 5'-TGCTGGAAGGTGGACAGTGAGG-3'; *Syp*: 5'-TTCAGGAC-TCAACACCTCGGT-3' and 5'-CACGAACCATAGGTTGCCAAC-3'; *Scn1a*: 5'-CTTGAGCCCGAAGCTTGCT-3' and 5'-TCCTTCT-TCCACGCTGATTTG-3'; *Scn2a*: 5'-CATCGTCTTCATGATTC-TGCTCA-3' and 5'-GGTTTTTCGCTGCTCGATGTA-3'; *Scn8a*: 5'-CATCTTTGACTTTGTGGTGGTCAT-3' and 5'-TGACGGG-AATAGGGTCG-3'; *Pvalb*: 5'-CTGGGGTCCATTCTGAAGGG-3' and 5'-TTCAACCCCAATCTTGCCGT-3'; *Hcn1*: 5'-TGAAG-CTGACAGATGGCTCTT-3' and 5'-GAGTCGGTCAATAGCAA-CTGTCT-3') and 2.5-fold diluted synthesized cDNA (total volume of qPCR reaction 20 μL), by incubating for 3 min at 95°C, 40 cycles of 15 s at 95°C and 1 min at 60°C. Quantification was based on b-actin.

Biocytin Stainings

Slices containing cells that were previously filled with biocytin during patch-clamp recordings were washed three times for 20 min in phosphate-buffered saline (PBS-T-T) containing 137 mM NaCl, 2.7 mM KCl, 10 mM Na₂HPO₄, 1.8 mM KH₂PO₄, 0.05% Triton X-100 (Sigma), and 0.2% Tween-20 (Sigma). Subsequently, slices were incubated in a staining solution containing 0.01 mg/mL of Streptavidin-Cy3 (Sigma, RRID: AB_1948868) in PBS-T-T overnight at 4°C. On the following day, slices were washed three times with PBS for 10 min, incubated in DAPI (Sigma, 1.43 μM) solution for 5 min, and again washed three times with PBS for 10 min. Finally, slices were mounted on Superfrost Plus adhesion slides (Eprelia) with Fluoromount G (Thermo Fisher Scientific).

Confocal Imaging and Morphological Reconstructions

Neurons stained with Streptavidin-Cy3 were selected for confocal imaging if they exhibited sufficient fluorescent signal and overall morphology of a pyramidal cell. Cells were then scanned as a whole in *x*-, *y*-, and *z*-axis on an inverted confocal microscope (Zeiss LSM710 and Zeiss LSM980 Airyscan 2) with a ×40 oil immersion objective. Single stacks were imaged at a resolution of 1,024 × 1,024 with multiple tiles in the *x* and *y* direction and *z*-stacks at 0.66 μm thickness. Fluorophore Cy3 was imaged with a 561-nm laser and a 569–712 filter.

Using the complete confocal neuron scans, 3-D models of corresponding neurons were generated using the neuron tracing tool in Arivis software (Zeiss, RRID: SCR_018000). Axon, dendrites, and soma were segmented, and the obtained 3-D models of neurons were further used for morphological analysis.

Data Analysis and Statistics

Patch-clamp recording analysis.

Patch-clamp data were analyzed using Fitmaster software (HEKA, RRID: SCR_016233) and custom-written scripts for MatLab (MathWorks, RRID: SCR_001622). Cells were included in the analysis, when membrane potential was ≤ -60 mV, they were able to generate multiple action potentials upon current injection, and action potential amplitude was larger than 40 mV. In Fitmaster, data were filtered digitally at 1 kHz to remove artifacts. Action potentials were analyzed using the corresponding software function. The membrane potential was measured at the start points of every protocol and a mean value was calculated for every cell. Input resistance was determined by creating an *I-V* curve of current input responses in whole-cell mode and calculating the reverse slope value $\Delta V/I$. Spontaneous events in the current-clamp mode were characterized as starting by reaching rheobase (at least one spike) and ending if membrane potential returned to baseline for at least 500 ms. Spontaneous events in voltage-clamp mode were characterized by reaching an amplitude of at least 200 pA and ending if the current returned to baseline for at least 500 ms. Spontaneous events were analyzed using the corresponding functions in Fitmaster software. Several integral values that could not be calculated in Fitmaster due to baseline shift issues were subsequently calculated with a custom-written MatLab script. For all values corresponding to a

single event (duration, integral, spikes, positive/negative amplitude), mean values were created for every cell. ROUT method outlier test was performed and data were tested for normality and distribution via Shapiro–Wilk test. Significance in differences between time periods was calculated per GraphPad Prism 10 software (RRID: SCR_002798) using one-way ANOVA or mixed statistical test with post hoc Tukey's multiple comparisons test for normally distributed data. For data that was not normally distributed, analysis was done with Kruskal–Wallis statistical test and Dunn's multiple comparison correction.

MEA analysis.

MEA recordings were analyzed using custom-written Matlab (MathWorks, RRID: SCR_001622) scripts. For each slice, two recording epochs of 5 min and (if present) three network-driven local field potentials (LFPs) per recording were analyzed. The data were first filtered with a low pass filter of 50 Hz and, if present, noisy channels were removed from the analysis. LFP events were detected at individually selected thresholds per recording in a manually chosen reference channel. An individual time window was subsequently set for the analysis of an LFP event. In the first step, we qualitatively judged the complexity of the LFP as 1) very low, 2) low, 3) medium, 4) complex, or 5) very complex. Categorization criteria for waveform analysis were as follows: one single spike (very low), 2–3 spikes (low), >3 spikes (medium), initial spike followed by high-frequency oscillation at a low amplitude not reaching the initial amplitude (complex), high-frequency oscillation at a high amplitude reaching the full initial amplitude (very complex), or not applicable (n.a.), when the waveform did not fall into one of the categories. Subsequently, the average of the minimum and maximum amplitudes over all channels throughout the recording was calculated. The threshold was set for positive and negative LFP components as a value between 5 and 20% above or below the average value. Afterward, the electrodes that crossed the threshold values at least once within the selected recording period were counted as active electrodes. From the number of active electrodes, we further calculated 1) a ratio of positive versus negative electrodes (note that an electrode could be both positive and negative if the signal crossed both thresholds during the period analyzed), 2) the propagation speed of positive and negative LFP components, 3) the average value of positive and negative LFP amplitudes (averaged over all active electrodes), and 4) duration of the LFP (averaged over all channels). Up to three LFPs per recording and two recordings per slice were analyzed, and all values depicted in graphs were averaged per recorded slice. In addition, one LFP per slice corresponding to the most dominant type of waveform for each time period was analyzed for frequency bands α (8–13 Hz), β (13–30 Hz), γ (30–150 Hz), and δ (1–4 Hz). This analysis was done by calculating the normalized power difference of frequency bands detected during the LFP event as compared with a control window of the same length without a LFP event. Significance in differences between time periods was calculated using one-way ANOVA or mixed statistical test with post hoc Tukey's multiple comparisons test for normally distributed data and Kruskal–Wallis statistical test with post hoc Dunn's multiple comparisons test for not

normally distributed data per GraphPad Prism 10 software (RRID: SCR_002798).

Immunohistochemistry analysis.

Per slice, two regions of interest were selected, one in the prefrontal cortex/secondary motor cortex and one in the somatosensory cortex. As no difference was found between those two regions, both regions of interest (ROIs) were counted and included in the analysis. Cell counting was automated and NeuN count was used as a normalizer at 100% to calculate the overall percentage of parvalbumin-positive cells. Mean values were generated for every slice and subsequently, for every time period. Significance in differences between time periods was calculated using one-way ANOVA statistical test with post hoc Tukey's multiple comparisons test per GraphPad Prism 10 software (RRID: SCR_002798).

Morphological analysis.

Neurons were reconstructed with the neuron tracing tool in Arivis software (Zeiss, RRID: SCR_018000). Dendrites were reconstructed from the soma to terminal endpoints and 3-D models of neurons were subsequently segmented into apical and basal dendrites. Values for dendritic length, branch points, and terminal end points were ascertained in Arivis software and plotted in GraphPad Prism 10 software (RRID: SCR_002798). The axon was not included in the analysis. Significance in differences between time periods was calculated using one-way ANOVA statistical test with post hoc Tukey's multiple comparisons test.

RESULTS

Development of Cellular Electrophysiological Properties in Organotypic Neocortical Cultures in Layer 2/3 Pyramidal Cells

For this study, we used organotypic brain slice cultures (oBSCs) generated from mice aged 5–6 postnatal days (P5–6) and targeted pyramidal cells of the somatosensory area of the cortex, located at a depth of 100–500 μm from the cortical surface. Pyramidal cells were identified during patch-clamp recordings by their somatic shape and general firing behavior, and post hoc by their morphology (Fig. 1A). Recordings were performed continuously from 2 days in vitro (DIV) up to 37 days in vitro with six time periods characterized as: initial (1–2 DIV), *week 1* (6–9 DIV), *week 2* (11–16 DIV), *week 3* (17–23 DIV), *week 4* (28–30 DIV), and *week 5* (34–37 DIV). Overall, 179 neurons were recorded and included in our analysis for periods initial ($n = 21$), *week 1* ($n = 28$), *week 2* ($n = 36$), *week 3* ($n = 45$), *week 4* ($n = 30$), and *week 5* ($n = 19$). In response to depolarizing current injection, we observed that neurons of the initial culturing period exhibited immature firing behavior and depolarization block after several action potentials, thus not being able to fire continuous trains of action potentials when depolarized into firing saturation (Fig. 1B, initial). Interestingly, this observation was resolved already during the first week in culture with neurons gaining and retaining the ability to fire continuous trains of action potentials up to 5 wk in culture (Fig. 1B, *week 1* to *week 5*). Although nearly two-thirds of recorded neurons displayed a depolarization block during the initial culturing

period, this phenomenon was only found occasionally during the later time points (Fig. 1C). Action potentials were broad during the initial culturing period and the first week with an action potential half-width of 2.6 ± 0.2 ms and 2.4 ± 0.1 ms, respectively, and decreased continuously during the following weeks to reach mature steady-state values of 1.9 ± 0.1 ms after 3 wk (Fig. 1D). The instantaneous firing frequency was slightly, but not significantly elevated during the initial culturing period with an area under the curve (AUC) value of 269.3 ± 31.0 but decreased and stabilized during culturing *weeks 1* and *2* to a value of 124.5 ± 16.1 . Interestingly, this value significantly increased again at the later culturing periods to a final value of 528.8 ± 65.3 in *week 5* (Fig. 1E).

Another parameter for neuronal maturation in organotypic cultures was found in the voltage sag, defined as the ratio between the steady-state decrease and the largest decrease in voltage following a hyperpolarizing current, in this case -200 pA. The sag is caused by hyperpolarization-activated cation current (I_h) and is thought to be mainly controlled by the activation of hyperpolarization-activated cyclic nucleotide-gated (HCN) channels (44). The voltage sag was significantly elevated during the initial culturing at 9.1 ± 1.0 mV, but decreased and reached steady-state levels at *week 1* with 3.1 ± 0.5 mV (Fig. 2A and Fig. 3C).

The cellular input resistance displayed a similar development over time with values significantly elevated during initial culturing at 338.2 ± 29.2 M Ω , followed by a decrease and stabilization after 1 wk to 168.0 ± 9.9 M Ω (Fig. 2, B and C). The resting membrane potential resided at -73.7 ± 1.0 mV in the initial culturing phase and underwent significant hyperpolarization by *week 2*, dropping to -81.2 ± 1.7 mV (Fig. 2D). All individual values are given in detail in Supplemental Table S1.

Overall, our data suggested a generally immature neuronal phenotype shortly after culture production from mice aged 5–6 postnatal days, but also continuing maturation during the first 3 wk in vitro to a more stabilized state with increasingly mature firing behavior and intrinsic excitability.

Development of Spontaneous Activity in Organotypic Neocortical Cultures

We first wanted to observe spontaneous activity in organotypic cultures on a single-cell level and therefore monitored events in current-clamp mode during whole-cell patch-clamp recordings over our culturing periods initial ($n = 17$), *week 1* ($n = 25$), *week 2* ($n = 30$), *week 3* ($n = 36$), *week 4* ($n = 23$), and *week 5* ($n = 17$). This data set contained fewer cells than the previous one, as recordings of spontaneous activity were not performed for every cell. Spontaneous activity in current-clamp mode was characterized as an "event" when it reached the action potential threshold at least once and was considered as finished when it returned to baseline afterward for at least 500 ms (Fig. 3A).

We evaluated a recording time of 3 min for every cell and calculated mean values for every parameter corresponding to single events, such as duration, action potentials per event, and integral. We observed a striking increase in the number of events and event duration over the cultivation period of 5 wk, with neurons exhibiting nearly no spontaneous

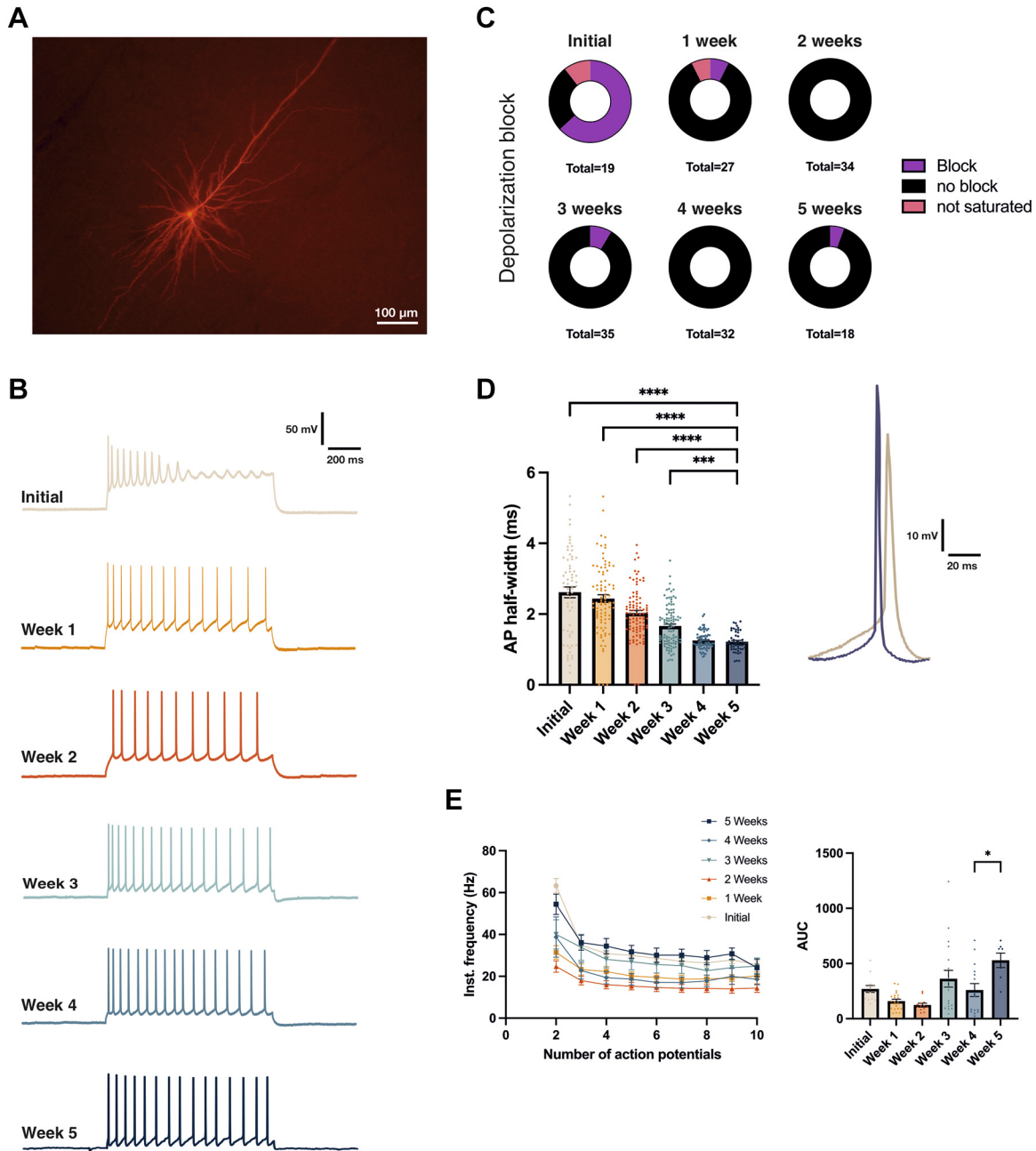
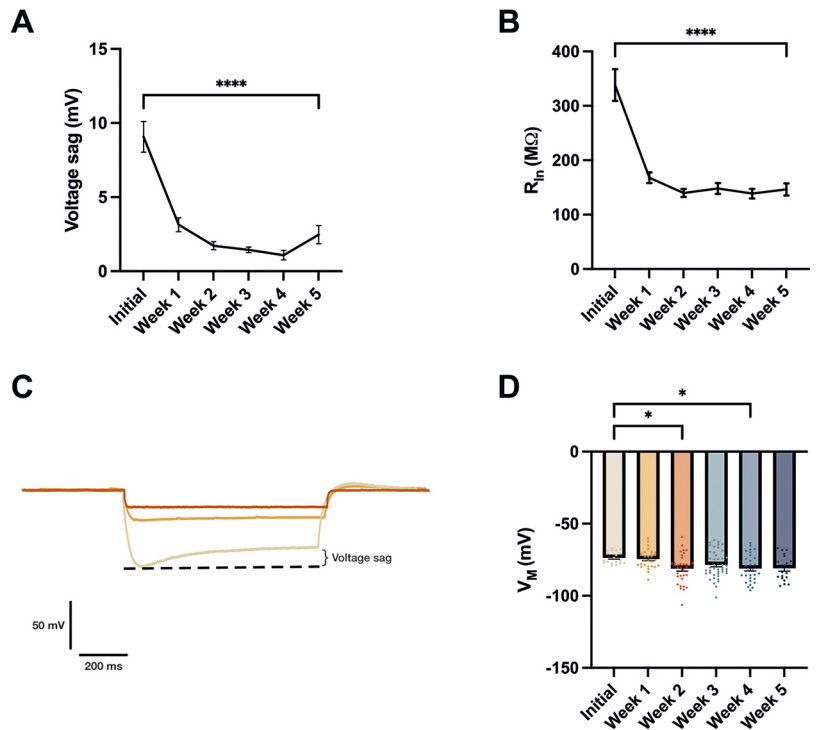


Figure 1. Firing properties of recorded neurons. **A:** exemplary pyramidal cell, biocytin filled during patch-clamp recordings and stained with Streptavidin-Cy3, 16 days in vitro (DIV). **B:** examples of induced spike trains from pyramidal cells of every time period, ~100 pA above rheobase. **C:** illustration of the proportion of neurons exhibiting depolarization block upon current injection until saturation of the number of action potentials. **D:** development of action potential half-width over a time course of 5 wk. Visual comparison of action potential width between the initial culturing period and 5 wk in vitro. **E:** development of instantaneous firing frequency over 5 wk of cultivation, the area under the curve illustrated in the graph on the right. For all graphs: **** $P < 0.0001$, *** $P < 0.001$, * $P < 0.05$ for Kruskal–Wallis test.

activity during the initial culturing phase and becoming gradually more active over time. The mean duration of spontaneous events increased from short bouts of activity to more complex and elaborate activity patterns that still contained single spikes and short events, but also cellular up-states. This resulted in a significant increase in the mean duration of events between the initial culturing period, where events displayed a mean duration of 0.3 ± 0.2 s, and the following time periods, with a mean duration of 2.4 ± 0.4 s at week 2 and 8.0 ± 4.7 s at week 5 (Fig. 3B). The development of

spontaneous activity is best illustrated by the exemplary traces shown (Fig. 3C), showing the mostly silent state of initial cultures (Fig. 3C, initial) progressing to up-states exhibiting only a few action potentials and partial depolarization block (Fig. 3C, week 1) to elaborate spontaneous events accompanied by prolonged bursts of action potentials during later cultivation periods (Fig. 3C, weeks 2, 3, and 4). Interestingly, several neurons started displaying abnormal forms of excitatory discharges at week 5 in culture (Fig. 3C, week 5), however, it has to be stressed that these high-

Figure 2. Passive properties and voltage sag of recorded neurons. *A*: development of voltage sag over 5 wk. *B*: development of input resistance over 5 wk. *C*: comparison of input resistance and voltage sag between neurons of *initial*, *week 1*, and *week 2* culturing periods. *D*: development of resting membrane potential over a time course of 5 wk. Significance levels for all graphs: * $P < 0.05$, **** $P < 0.0001$ for Kruskal–Wallis test.



frequency events were not the exclusive or dominating form of spontaneous activity and were only rarely observed in cultures aged 4–5 wk (Supplemental Fig. S1). This is also highlighted by the fact that spontaneous activity did not seem to continuously accelerate into a high-frequency phenotype during culture as shown by the overall number of events per cell, with on average 0.9 ± 0.5 events observed per 180 s in the initial culturing period and stable values of 9.0 ± 1.5 events by *week 2* (Fig. 3D). This was also reflected by the active time spent above resting membrane potential, increasing from $0.5 \pm 0.3\%$ at initial culturing periods to a steady-state value of $11.8 \pm 2.5\%$ by *week 2* (Fig. 3E). These activity parameters only showed a significant increase when comparing the initial culturing phase to later culturing periods, but no continuous increase in-between later periods. Instead, spontaneous activity shifted to more complex patterns composed of single spikes, bursts, and long-lasting up-states. The absolute number of action potentials recorded per cell over a period of 3-min recording time significantly increased after the initial culturing from 1.2 ± 0.6 to 63.7 ± 18.6 at *week 2*, stayed stable until *week 4* and subsequently showed a trend toward increasing further in *week 5* to 108.2 ± 64.2 (Fig. 3F). The change between the proportions of different types of spontaneous activity was especially highlighted by the number of spikes per event, which saw a significant increase from initial values at 0.4 ± 0.2 to 4.9 ± 1.1 at *week 2*, but also a clear trend in late time periods toward spontaneous events encompassing larger numbers of action potentials with a final value of 25.1 ± 20.4 at *week 5* (Fig. 3G). This was further illustrated by calculating the integral for every event, resulting in values for the area under the curve in unit V·s, and comparing mean values between individual cells. The integral value increased significantly from 1.2 ± 0.9 V·s at the initial culturing phase compared with 66.2 ± 20.4

V·s at *week 3*, but the difference ceased to be significant in *week 4* and *5* despite values of 79.9 ± 50.4 V·s and 95.1 ± 75.5 V·s, respectively.

This was due to the activity of the neurons becoming more heterogeneous, resulting in a rise of variance and a clustering into cells exhibiting predominantly single spikes and short bursts versus cells that tended to display long, elaborate up-states, some of them potentially drifting into either high-frequency oscillations or runaway excitation and pathological activity. All individual values are given in Supplemental Table S1.

In summary, when looking at the intracellular spontaneous activity of the cell, cortical pyramidal neurons were nearly silent in the initial phase of cultivation but started to progressively develop spontaneous activity during the first 2 wk in culture (Fig. 4, *week 1*). For later cultivation time points, especially *weeks 4* and *5*, heterogeneity between individual cells and cultures rose, including all kinds of spontaneous activity patterns from near-silent, single spiking, and bursting activity to complex up-states (Fig. 4, *week 4*) and even discharge patterns that could be characterized as high-frequency oscillations or epileptiform activity (Supplemental Fig. S1).

To further evaluate how these patterns of spontaneous activity develop, we also analyzed voltage-clamp whole-cell patch-clamp recordings. Cells were included over the whole time course of the culturing periods, namely initial ($n = 14$), *week 1* ($n = 17$), *week 2* ($n = 21$), *week 3* ($n = 34$), *week 4* ($n = 23$), and *week 5* ($n = 17$). The development of synaptic input was coherent with the findings made in current-clamp recordings (Supplemental Fig. S2). Events gradually increased in frequency, length, and complexity over the culturing period, mirroring the development of spontaneous neuronal activity. The rise of inhibitory input

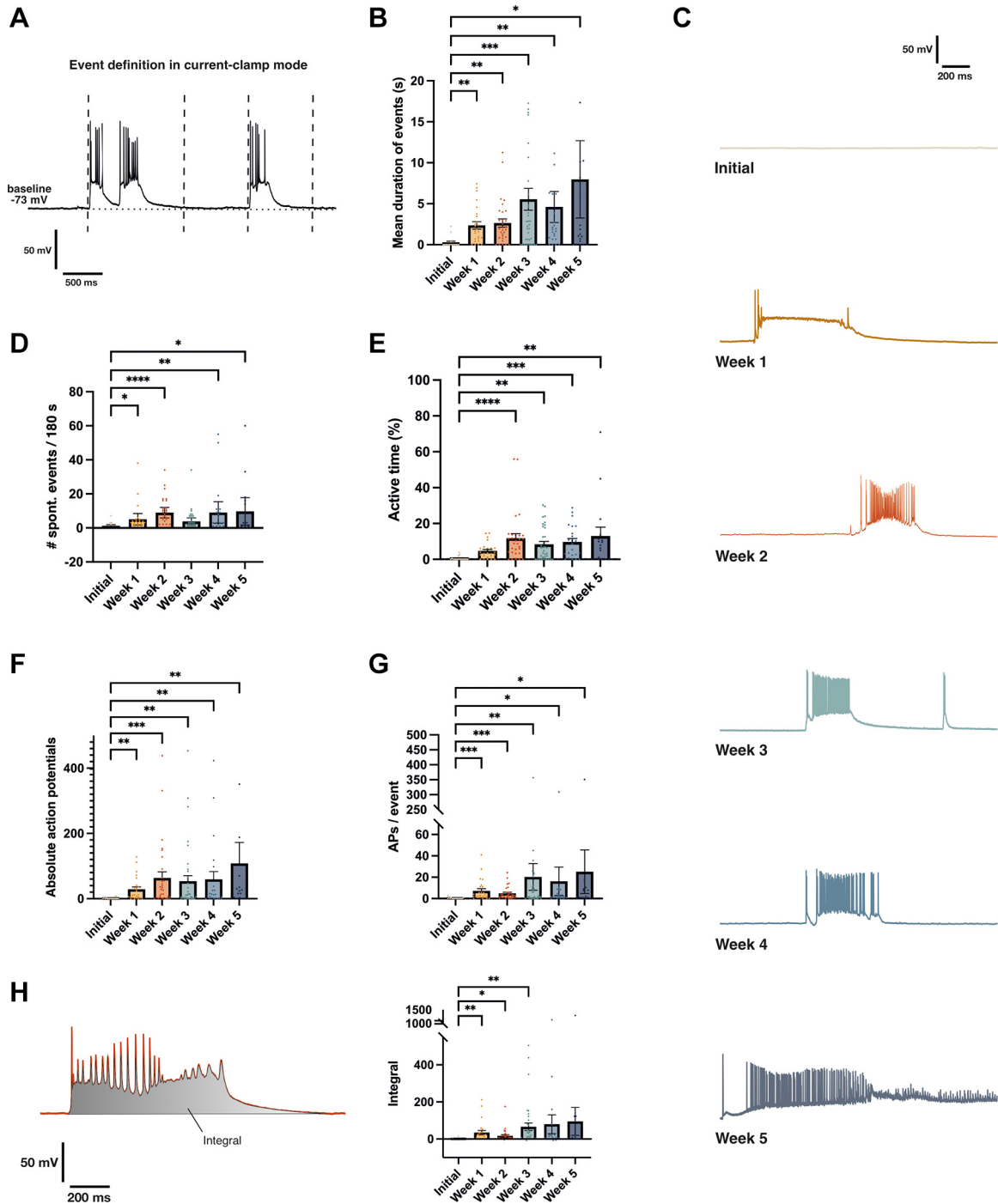


Figure 3. Spontaneous activity as recorded in current-clamp mode. *A*: definition of events during current-clamp recordings, event starting at reaching action potential threshold and ending when returned to baseline for at least 500 ms. *B*: mean duration of spontaneous events. *C*: exemplary traces of spontaneous up-states recorded. *D*: number of spontaneous events recorded per cell over a recording time of 3 min. *E*: percentage of recording the cell spent in an active state, meaning above baseline in an active event as defined in *A*. *F*: overall number of spontaneous action potentials recorded in one cell over a recording time of 3 min. *G*: number of action potentials per single event recorded. *H*: visual representation of the definition of integral as area under the curve of a spontaneous event with unit V·s. Graph illustrating numeric evaluation depicted on the right. Significance levels for all graphs: **** $P < 0.0001$, *** $P < 0.001$, ** $P < 0.01$, * $P < 0.05$ for Kruskal–Wallis test.

was observed with a slight delay to excitatory input and values became more heterogeneous and clustered into low- and high-activity profiles during culturing periods weeks 4 and 5. All individual values are given in the Supplemental Table S1.

Morphological Development of Neocortical Pyramidal Neurons in Culture

Next, we investigated the cellular morphology and its development over the culturing period in cells that were filled

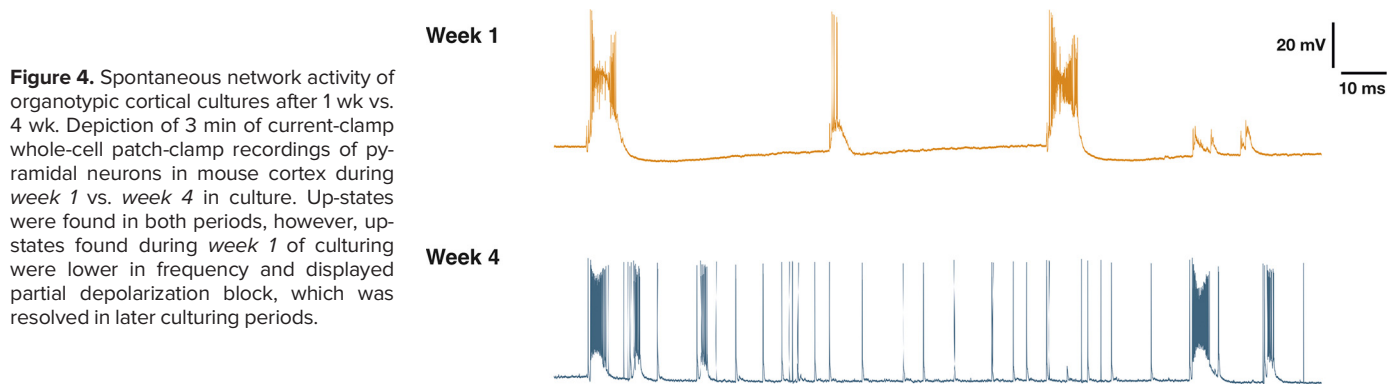


Figure 4. Spontaneous network activity of organotypic cortical cultures after 1 wk vs. 4 wk. Depiction of 3 min of current-clamp whole-cell patch-clamp recordings of pyramidal neurons in mouse cortex during *week 1* vs. *week 4* in culture. Up-states were found in both periods, however, up-states found during *week 1* of culturing were lower in frequency and displayed partial depolarization block, which was resolved in later culturing periods.

with biocytin during patch-clamp recordings. Cells were stained with Streptavidin-Cy3, imaged on a confocal microscope, and reconstructed (see MATERIALS AND METHODS for details). Per time period, we included five cells in the analysis (Supplemental Fig. S3).

All cells exhibited the typical morphological form of pyramidal cells (Fig. 5A) and were analyzed for their total dendritic length, number of branch points, and number of terminal endpoints. The total dendritic length of neurons increased significantly from $1,511.0 \pm 269.6 \mu\text{m}$ at the initial culturing phase up to $5,030.0 \pm 143.2 \mu\text{m}$ in *week 4* but significantly dropped to $3,310.0 \pm 286.4 \mu\text{m}$ between *week 4* and *week 5* (Fig. 5B). A similar development was observed for the number of total branch points, increasing from 24.4 ± 2.4 at initial culturing to 55.0 ± 3.9 by *week 2*, but dropping again to 37.8 ± 3.5 in *week 5* (Fig. 5C) and number of terminal endpoints, which significantly increased after the initial culturing phase from 34.2 ± 3.7 to 67.4 ± 4.0 by *week 2*, but decreased again to 49.0 ± 3.7 in *week 5* (Fig. 5D).

A coherent development was observed when apical and basal dendrites were analyzed separately (Supplemental Fig. S4). All individual values are given in the Supplemental Table S1.

In conclusion, these findings mirror the ongoing maturation of neurons after the initial culturing phase up to *week 2* of culturing and stability thereafter, but also again highlight the occurring changes in *week 5* of culturing.

Slice Culture Progression Is Coherent with In Vivo Postnatal Development

After we investigated the development of several main neuronal parameters in neocortical mouse brain cultures over 5 wk, we wanted to determine whether this development was comparable with postnatal development in vivo. For this purpose, we compared our data to the results of studies investigating the postnatal development of neurons in the mouse visual cortex (45), medial prefrontal cortex (46), and auditory cortex (47) in acute brain slices over the postnatal period. Postnatal days were compared with days in vitro with the initial age of euthanized mice added ($P6 + \text{days in vitro} = \text{postnatal days}$). Strikingly, the development of intrinsic properties such as resting membrane potential and input resistance closely resembled the in vivo development in other cortical areas (Fig. 6, A and B). The action potential half-width was slightly shorter in neurons recorded

in acute slices compared with cultured neurons, and developed more slowly than in vivo, reaching steady-state values by *week 4* in culture, comparable with 35 postnatal days, whereas steady-state in the living animal was already reached at *postnatal day 14–28* in comparable studies (Fig. 6C). The morphological development of the dendritic arborization of the neurons in culture was on par with the progression of total, apical, and basal dendritic length as seen in vivo (Fig. 6, D–F). In conclusion, pyramidal neurons in the somatosensory area of cultured neocortical mouse brain slices develop normally in terms of morphology and intrinsic electrophysiological features and closely resemble in vivo development up to 3 wk in culture.

Network Dynamics of Neocortical Organotypic Brain Slice Cultures Show a Transition to High-Frequency Oscillatory Phenotype

Considering our findings on the single-cell level, we were wondering how the development of spontaneous activity would reflect on a network level. Therefore, to get more insights into the overall network activity of our cortical cultured slices over time in vitro, we performed multi-electrode array (MEA) recordings for every time period, namely $n = 17(9)$ for initial, $n = 17(9)$ for *week 1*, $n = 7$ for *week 2*, $n = 8$ for *week 3*, $n = 8$ for *week 4*, and $n = 7$ for *week 5*, $n = \text{number of slices}$. Recordings were performed on a 16×16 (256) electrode grid and the slice was positioned in a way that would cover the somatosensory cortical area. Afterward, recordings were analyzed using custom-written Matlab scripts (see MATERIALS AND METHODS for details) detecting every electrode that reached the individual threshold for positive or negative components of local field potentials (LFPs) and calculating their corresponding amplitudes (Fig. 7A, top row).

As all slices displayed robust network-driven LFP activity covering all neocortical portions, we chose reference channels with the highest amplitude for every recording to analyze a maximum of three LFPs per recording. Our analysis scripts detected onset and termination points for each LFP and calculated their individual amplitudes, timeframes, and waveforms (Fig. 7A, bottom row). Subsequently, we analyzed which waveforms of LFPs were the most dominating throughout the slices at different time points. We found mostly simple waveforms for the initial culturing phase, consisting of merely one positive and one negative component,

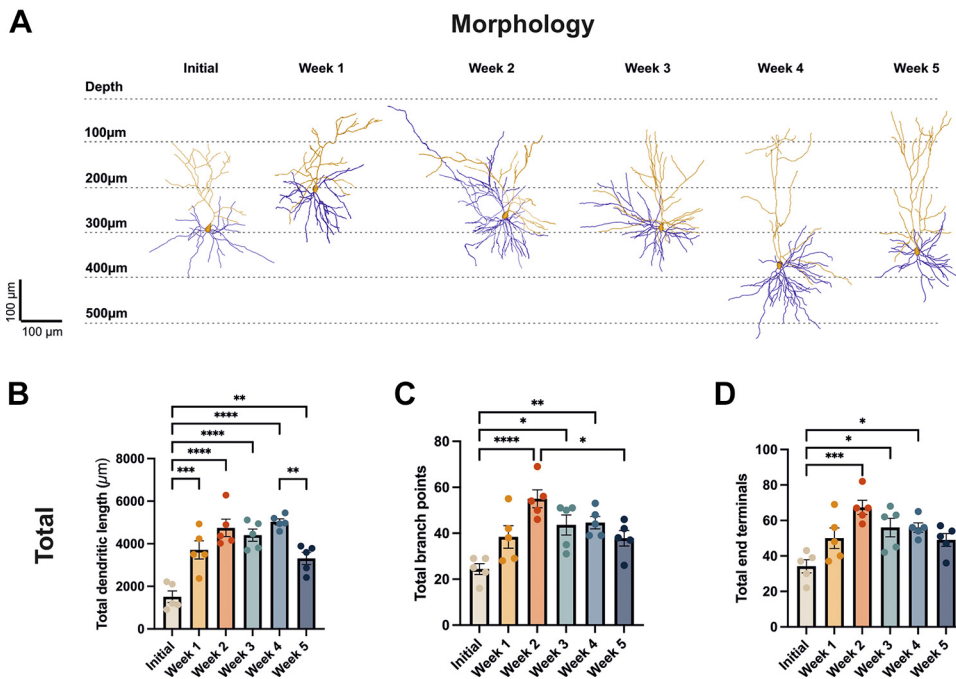


Figure 5. Development of pyramidal cell morphology. *A*: representative reconstructions of neurons for each culturing period, depicted at their corresponding depth as measured from the cortical surface. Apical dendrite is color-coded in orange, basal dendrites in blue. *B*: graph depicting the development of total dendritic length over the culturing periods. *C*: graph depicting the development of the number of total branch points over the culturing periods. *D*: graph depicting the development of the number of total dendritic end terminals over the culturing periods. Significance levels for all graphs: * $P < 0.05$, ** $P < 0.01$, *** $P < 0.001$, **** $P < 0.0001$ for one-way ANOVA test.

followed by maturing of the activity pattern into more elaborate waveforms encompassing a higher number of different components throughout culturing in *week 1*, *week 2*, and *week 3*, but shifting into multiple seconds long, oscillating events in *week 4* and *week 5* (Fig. 7B). Though LFP waveforms were more of a spectrum rather than clearly distinguishable subtypes, it appeared like patterns of certain complexities were dominating each culturing period. Hence,

to give a better overview of which type of LFP is dominating which culturing period, we classified LFP waveform complexity by spike number and pattern, with one spike defined as consisting of both positive and negative components. LFPs were classified into complexities very low (single spike), low (2–3 spikes), medium (>3 spikes), complex (initial spike(s) followed by low amplitude oscillation, not reaching amplitude of initial spike), and very complex

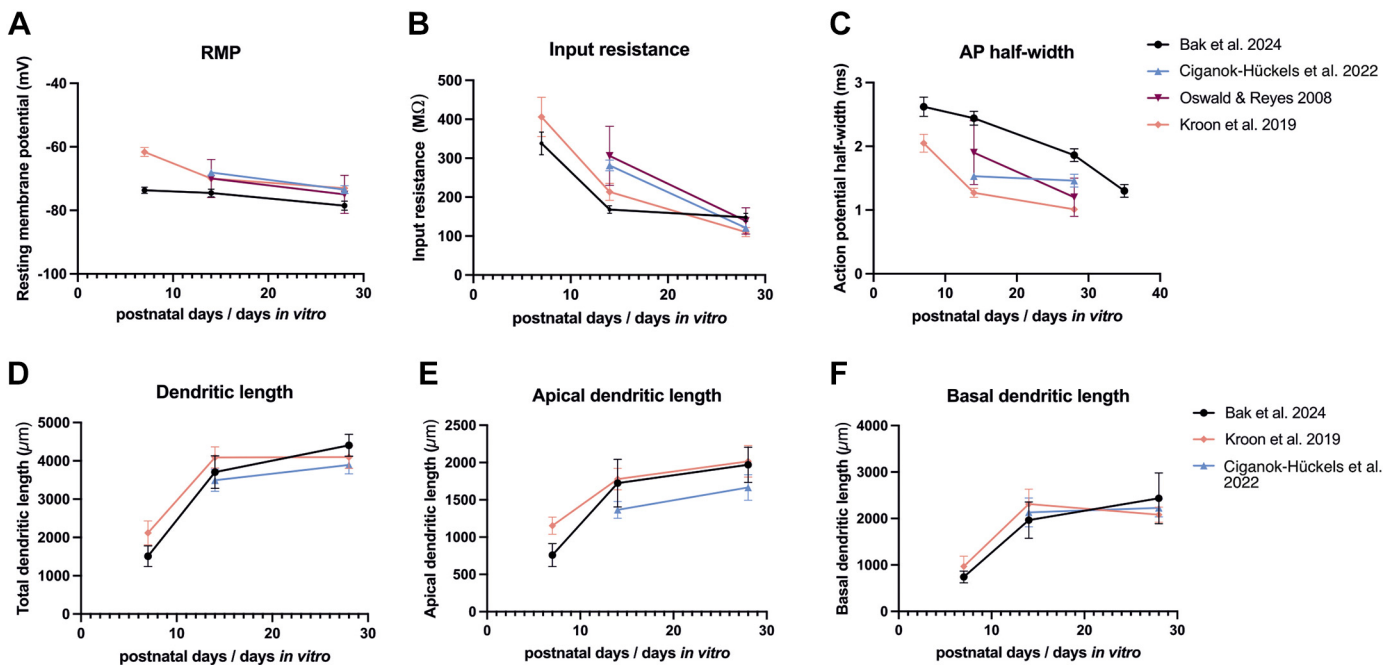


Figure 6. Comparison of organotypic brain slice culture development to the *in vivo* situation. Data obtained from cultured mouse neocortex was compared with data from other studies, obtained from acute slices at comparable time points concerning postnatal days/days *in vitro*. Data presented in this study is depicted in black, data from other studies is depicted in color. Comparison depicted for resting membrane potential (*A*), input resistance (*B*), action potential half-width (*C*), total dendritic length (*D*), apical dendritic length (*E*), and basal dendritic length (*F*).

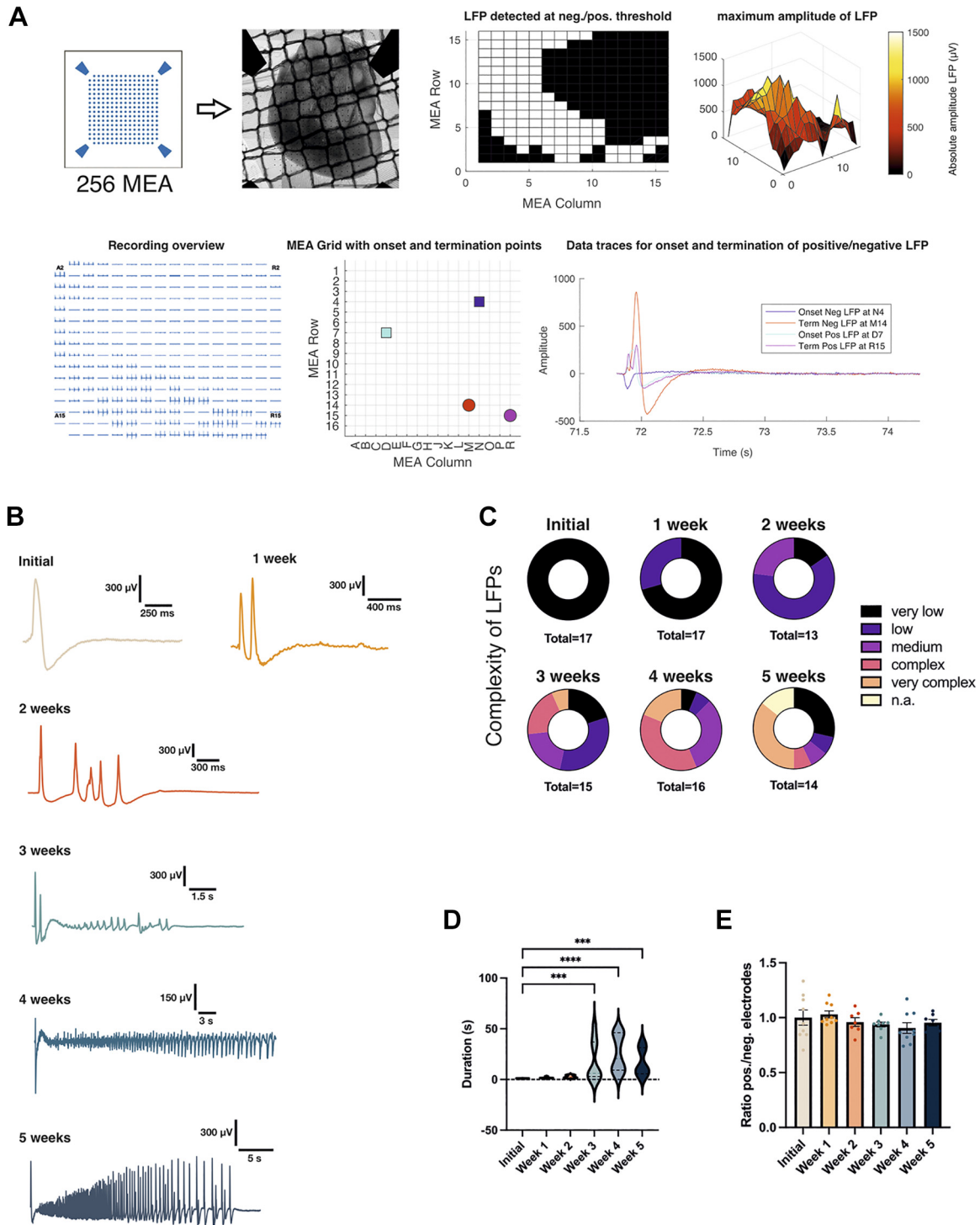


Figure 7. Multielectrode array (MEA) recordings of organotypic cultures. **A:** schematic representation of MEA recording and analysis pipeline. Slices were positioned on 16×16 (256) electrode grid to cover the somatosensory cortical area. Every slice was recorded for 2×5 min and from each recording, three local field potentials (LFPs) were analyzed at most. During analysis, electrodes reaching threshold for either positive or negative components of LFPs were detected and maximum amplitude was calculated. The specific LFP was analyzed from one reference channel, representative of activity seen in the remaining electrodes as illustrated in the overview of the recording. Onset and determination points of positive and negative components were detected and the waveform of the individual LFP was generated. **B:** exemplary waveforms of LFPs over a time course of 5 wk. **C:** development of LFP complexity over 5 wk with LFPs categorized into very low (single spike), low (2–3 spikes), medium (4–5 spikes), complex (1–3 initial full-sized spikes followed by low amplitude oscillation), and very complex (initial spike followed by full-sized amplitude oscillation). **D:** mean duration of LFPs for every recording over 5 wk, $***P < 0.001$ and $****P < 0.0001$ for Kruskal–Wallis test. **E:** ratio of electrodes reaching positive vs. negative threshold for every recording obtained.

(initial spike(s) followed by high amplitude oscillation, reaching full amplitude of initial spike).

Although in the initial culturing phase, exclusively LFPs of very low complexity were observed, and LFP waveforms seemed to follow a similar maturation course as observed in the other experiments. LFPs became more elaborate up until *week 3* of culturing, however, complex (37.5%) and very complex (31.25%) oscillating events were taking over and dominated over half of the recordings performed by *week 4* (Fig. 7C). Interestingly, while events of very low complexity only made up small proportions from *week 2* to *week 4*, they suddenly reappeared as one of the dominating components in *week 5* (28.57%) along with very complex oscillating events (35.71%), again illustrating the increasing heterogeneity of the cultures and their clustering into groups of low/medium basal activity and high activity, especially during *week 5*. This was also reflected in the duration of events, which significantly increased from 1.0 ± 0.1 s at the initial culturing phase to 17.9 ± 7.0 s in *week 3* and 25.5 ± 6.1 s in *week 4*, but also showed distinct clustering into shorter and longer durations from *week 3* to *week 5* (Fig. 7D), resulting in a decreased mean duration of 16.9 ± 4.8 s in *week 5* because of a cluster of slices exhibiting simple, short waveform LFPs as seen before in Fig. 7C.

Comparison of the ratio between electrodes reaching threshold for either positive or negative components of the LFP remained stable with no significant differences (Fig. 7E), indicating there were always both elements to every LFP. We then analyzed the amplitude of both positive and negative LFP components per detected LFP (Supplemental Fig. S6, A and B) and averaged the values per recorded slice to obtain quantitative data on LFP development. The average negative LFP amplitude increased from -0.2 ± 0.1 mV to -0.5 ± 0.1 mV by *week 4* (Supplemental Fig. S6C) and the average positive LFP amplitude increased from 0.3 ± 0.6 mV to 1.4 ± 0.3 mV by *week 4* (Supplemental Fig. S6D). Interestingly, changes in average LFP amplitude gradually increased over the whole culturing period, but only became significant between the initial culturing phase and *week 4*, due to the occurrence of oscillations including increasingly larger spikes. All individual values are given in Supplemental Table S2. Furthermore, we analyzed LFP propagation parameters such as propagated distance and propagation speed by evaluating the time course of single electrodes crossing LFP threshold (Supplemental Fig. S6, E and F), however, no significant differences were found (Supplemental Fig. S6, G and H).

Finally, we analyzed the frequency bands by comparing the frequencies detected during LFP events to baseline control regions without LFP events. Frequency bands were separated into α (8–13 Hz), β (13–30 Hz), γ (30–150 Hz), and δ (1–4 Hz), and the normalized power difference of the event region was analyzed per recorded slice as compared with the baseline control region.

Alpha (α) and β frequency bands significantly increased by *week 1* in culture from 7.2 ± 1.9 dB to 16.9 ± 1.6 dB and 4.2 ± 1.2 dB to 16.5 ± 0.6 dB, whereas γ frequency bands were only detected from *week 3* onward, rising from 1.2 ± 0.5 dB during the initial culturing phase to 7.6 ± 0.9 dB by *week 3*, coherent with the appearance of increasingly complex high-frequency oscillations. No significant differences were found

in the δ frequency band, which was present throughout the whole culturing period, corresponding to the persistent presence of slow network oscillations with simple waveforms (Fig. 8A). The development of frequency bands during late culturing periods *weeks 4* and *5* shows a general trend of decline in all analyzed frequency bands, coherent with the trend observed in other parameters. During *week 5*, frequencies could not be detected as evenly distributed over the electrode grid covering the cortical area as it was seen before in earlier culturing periods (Fig. 8B).

Summarized, the MEA data confirmed the maturation of spontaneous network activity into more elaborate patterns from *week 1* to *week 3* of organotypic neocortical cultures, but also the increase of heterogeneity and variability accompanied by the appearance of high-frequency oscillations in *week 4* and *5*.

Development of the Expression of *Syp*, *Pvalb*, *Hcn1*, *Scn1a*, *Scn2a*, and *Scn8a* in Neocortical Organotypic Cultures

To gain more insight into the cellular development of cortical oBSCs, we extracted RNA from whole hemispheres cultured as organotypic brain slices. We examined the expression levels of synaptophysin as a general neuronal marker, and parvalbumin as a marker for fast-spiking interneurons. In addition, we analyzed the expression levels of *Hcn1*, *Scn1a*, *Scn2a*, and *Scn8a* to investigate the development of ion conductance. Tissue was collected at 2 DIV ($n = 7$), 7 DIV ($n = 7$), 14 DIV ($n = 6$), 21 DIV ($n = 8$), and 28 DIV ($n = 6$) respectively. Quantitative RT-PCR revealed that synaptophysin expression levels showed a trend of slight increase after the initial culturing period up until *week 2*, and showed a trend to decline between *week 2* and *week 4* (Fig. 9A), indicating first signs of neuronal loss, though not significant. Parvalbumin expression increased significantly between the initial culturing period and *week 3*, but also showed a trend to decrease toward later culturing periods (Fig. 9B). *Hcn1* showed a trend of increasing expression between the initial culturing and *week 3*, decreasing again at later time points (Fig. 9C). *Scn1a* and *Scn8a* expression increased significantly between initial culturing and *week 3* with a declining trend afterward (Fig. 9, D and F).

The expression curve for *Scn2a* showed high variability and was inconclusive, however, it appeared like *Scn2a* expression peaked in *week 1* of culturing, but subsequently decreased and stabilized at lower levels during *week 2* to *week 4* (Fig. 9E). Especially parvalbumin showed a clear elevation in expression between the initial culturing phase and *week 3*, with a nearly 20-fold increase in expression levels. We therefore decided to perform histological stainings on tissue sections of acute samples and cortex cultured for 7, 14, and 21 days respectively, and label for NeuN and parvalbumin.

Although the general cellular and neuronal content of slices largely persisted as demonstrated by DAPI and NeuN labeling, we observed a clear upregulation of parvalbumin-positive cells during *week 1* and *week 2* (Fig. 10A). This development was followed by a significant decline of the proportion of parvalbumin-positive neurons between *week 2* and *week 5* as seen in RT-PCR, but interestingly, already seemed

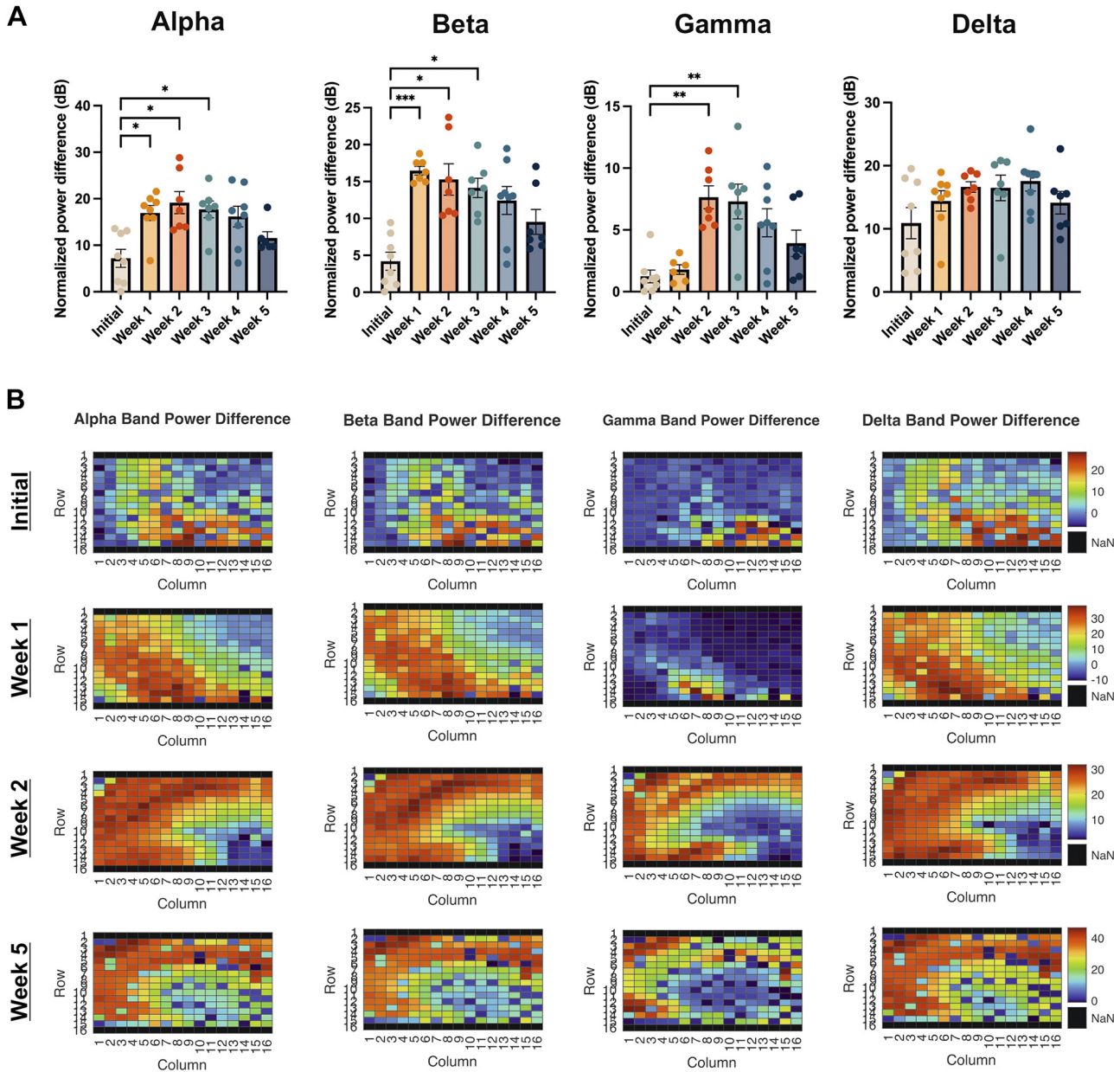


Figure 8. Evaluation of frequency bands in multi-electrode array recordings of organotypic cultures. Normalized power difference of detected α , β , γ , and δ frequency bands within local field potential (LFP) events as compared with baseline recordings without LFP event over the time course of 5 wk (A), exemplary heat map depiction of normalized power difference in frequency bands on the electrode grid of the multi-electrode array (MEA), illustrated for time points *initial*, *week 1*, *week 2*, and *week 5* (B). Significance levels for all graphs: *** $P < 0.001$, ** $P < 0.01$. * $P < 0.05$ for Kruskal–Wallis test.

to start during *week 3* (Fig. 10B). To ensure the specificity of the staining, we obtained confocal images of the stained tissue section (Fig. 10C). The general neuronal cell count did not significantly change throughout the whole culturing period (Fig. 10D), however, there was a trend of neuronal decline from *week 3*, consistent with the decline of parvalbumin-positive cells and other parameters. Moreover, cellular markers enriched in layer 5 (Ctip2) and layer 6 (Tle4) were consistent throughout the culturing (Supplemental Fig. S7), indicating that layer arrangement remained intact in cultured slices. All individual values are given in Supplemental Table S2.

In conclusion, RT-PCR and staining results indicated a clear upregulation of the markers parvalbumin, *Hcn1*, *Scn1a*, and *Scn8a* between the initial culturing phase and *week 3*.

Synaptophysin expression remained mostly stable, whereas *Scn2a* expression peaked in *week 2* and declined afterward. Nevertheless, nearly all markers dropped in expression by *week 4*, potentially indicating a general neuronal loss in late culturing phases *week 4* and *week 5*. Our stainings confirmed a significant neuronal loss of parvalbumin-positive cells and a beginning trend of overall neuronal cell count during late culturing periods.

DISCUSSION

The development of the early postnatal mouse neocortex in vitro concerning electrophysiological properties, morphology, and RNA expression levels holds important implications for the

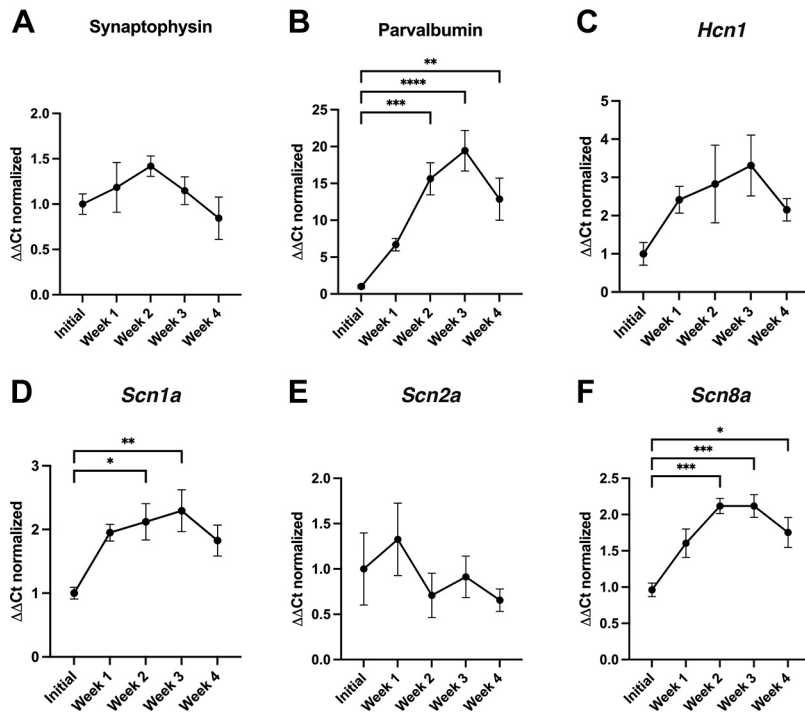


Figure 9. RT-PCR of markers synaptophysin, parvalbumin, *Hcn1*, *Scn1a*, *Scn2a*, *Scn8a*. Graphs depicting values for RT-PCR to evaluate development of RNA expression, namely synaptophysin (A), parvalbumin (B), *Hcn1* (C), *Scn1a* (D), *Scn2a* (E), and *Scn8a* (F), all values for initial culturing period normalized to 1, expression levels of following periods all normalized in relation to values of initial phase. Significance levels for all graphs: **** $P < 0.0001$, *** $P < 0.001$, ** $P < 0.01$, * $P < 0.05$ for one-way ANOVA.

planning of experiments involving mouse cortical oBSCs. When generating these cultures from postnatal P5–6 mice, we observed significant changes in the neuronal and network properties over 5 wk in culture. During the initial culturing phase, neurons displayed immature firing behavior characterized by a depolarization block and incomplete trains of action potentials. In the developing cortex, an increased input resistance along with a slow membrane time constant allows for the summation of excitatory postsynaptic potentials despite low network firing frequencies during the early developmental stages of the cortex (48). During the first week in culture, neurons matured and intrinsic properties and firing behavior became increasingly mature as demonstrated by significantly decreasing resting membrane potential, voltage sag, input resistance, and action potential (AP) half-width, closely mimicking the development in vivo (45, 49). Especially the progression of dendritic length and parameters such as resting membrane potential and input resistance were on par with the development seen in vivo when compared with studies in acute slices from equivalent ages in the auditory (47), visual (45), and prefrontal cortex (46), whereas the action potential half-width reached the reported mature values with ~ 1 wk of delay when compared with the alive animal. This maturation was also previously described in hippocampal cultures, accompanied by an increasing expression of synaptophysin (37). Intrinsic and firing parameters were probably hugely influenced by the ion conductance dynamics of the neurons, as RNA expression levels showed a continuous increase of *Hcn1*, *Scn1a*, and *Scn8a* expression levels between the initial culturing phase and week 3, which is also observed in vivo (50–52). Particularly the expression of sodium channels, which plateaus at week 2, is coherent with the development of the capability of neurons to produce elaborate up-states accompanied by repetitive firing of action potentials. The mismatch between the rise in *Hcn1* transcripts and the inversely proportional

decline of the voltage sag could be explained by several factors. First, the lysates used for the RT-PCR analysis originated from whole hemisphere slices, whereas electrophysiological evaluation was concentrated on the somatosensory area of the cortex. Second, these results could reflect the elevated early expression of other *Hcn* isoforms such as *Hcn2* and *Hcn4*, which have been shown to be expressed at manifold levels compared to *Hcn1* in thalamic neurons during the immediate postnatal period (53). The changes in ion conductance were furthermore reflected by the development of spontaneous activity, which was very rare on single-cell level in the initial culturing phase and increased over time in culture. Neurons gradually shifted from simple single spikes and short bursts to complex patterns of activity, containing elaborate up-states. This development of spontaneous activity in cultures of the somatosensory cortex along with the significant variability was described previously (39). It is also coherent with the rise in *Hcn1* expression levels, as *Hcn* channels have been found to influence bursting behavior (54). These results were also reflected by the phenomenon found in current-clamp events, where cells clustered into groups of medium or low activity and high activity, highlighting the heterogeneity of organotypic neocortical cultures in culturing week 4 and week 5. The variability of spontaneous activity on single-cell level could be attributed to the fact that network activity has been found to be initiated in L5 (55) with information in L2/3 being more sparse, variable, and informative (56). To analyze the network properties of the slice cultures, we measured activity using a 256 MEA system and focused on recurrent network events, which correlate with the spontaneous activity detected in the current clamp recordings of layer 2/3 pyramidal neurons. The network events in the MEA were analyzed using a threshold-based detection method (based on the mean of all channels) to identify active electrodes after applying a low-pass filter to the signals of all channels. We used a flexible

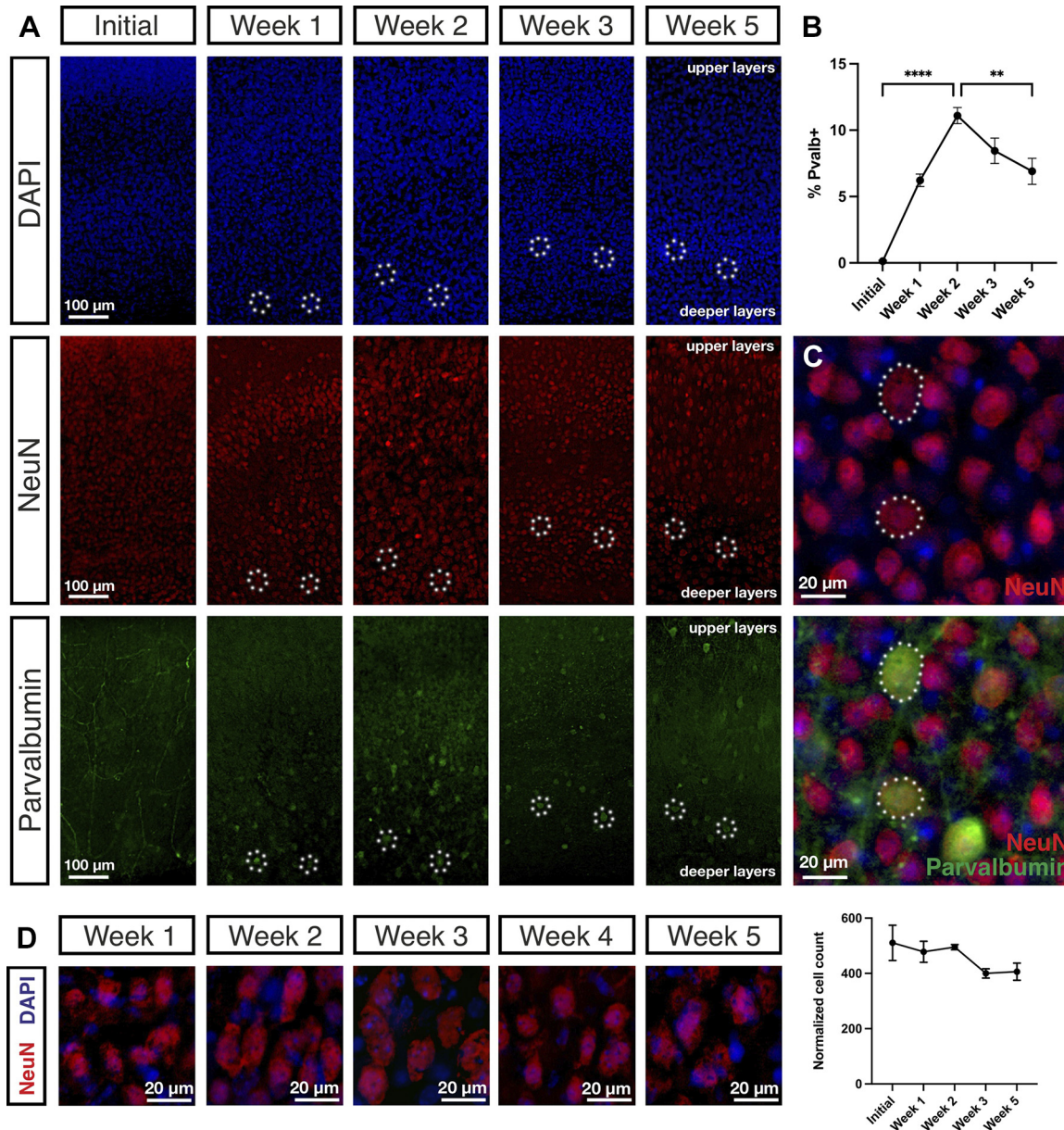


Figure 10. Development of parvalbumin-positive fast-spiking interneurons and neuronal cell count in organotypic cultures. **A:** stainings of cultures fixed at *initial*, *week 1*, *week 2*, *week 3*, and *week 5* time periods, namely DAPI, NeuN, and parvalbumin. **B:** graph depicting the development of the parvalbumin-positive neuronal population over time. **C:** specificity of parvalbumin staining as shown by confocal images of parvalbumin-positive neurons, which were simultaneously positive for NeuN. **D:** exemplary images of NeuN-positive cell density of culturing periods *week 1*, *week 2*, *week 3*, *week 4*, and *week 5* and graph depicting the development of normalized cell count of NeuN-positive cells over the whole culturing period. Significance levels for all graphs: $**P < 0.01$, $****P < 0.0001$ for one-way ANOVA test.

threshold-based approach on the average voltage signal, as our experience showed this method provided the most reliable results, minimizing false positives and false negatives in the detection of LFP components in the MEA recording. Network activity was present in all culturing phases, however, developed from a simple and short LFP waveform to high-frequency oscillations lasting multiple seconds by *weeks 4* and *5*. It is questionable whether these events can be categorized as pathological and epileptogenic, or if they are physiological oscillations. Considering the steep increase of parvalbumin expression levels by 20-fold as compared between the initial culturing phase and *week 3*, equivalent to the development seen in hippocampal

cultures (57) and in vivo (58), and the retained regularity of these events (Supplemental Fig. S5), it is likely that they were not caused by runaway excitation. The oscillations observed during MEA recordings had a controlled and rhythmic character, different from the aberrant activity found in few single-cell recordings or the epileptiform phenotype described after 4 wk in hippocampal cultures (11). Furthermore, slow δ oscillations were found to be constantly present throughout the whole culturing period, whereas α and β oscillations only occurred from *week 1* onward and γ oscillations were only found from *week 2* onward. Up-states and network oscillations both rely on a delicate balance between excitation and inhibition, which only

developed over time in culture, raising the possibility that the observed oscillations could be physiological. It has been shown that parvalbumin-positive neurons are crucial for the initiation of γ oscillations (59) and phase-lock to different oscillations in the hippocampus (60), whereas their loss leads to a decrease in overall oscillation and especially γ rhythm (61). This is consistent with the result that γ oscillations were predominantly found in *week 2* of culturing with a subsequent trend of decline, matching the levels of parvalbumin found in RT-PCR and stainings. As high-frequency network events were also terminated in a controlled manner, this indicates balanced excitatory and inhibitory forces. The maturation of single-cell and network properties in general happened independently from sensory input and therefore had to be driven intrinsically. This was also observed in sensory-deprived animals, where maturation onset happened with a delay of several days, but with the same time course (62). External electrical stimulation influences the frequency and distribution of spontaneous activity, and the proportion of up-states (26). Hence, it is likely that the deprivation of external input in oBSCs is balanced by an increase in spontaneous network activity and overall excitability as observed in visually deprived animals (63), which would explain the overall increase in excitability in culturing *weeks 4* and *5* despite the network reaching a mature state by *week 2*. This alteration of network properties to promote excitability as a response to the loss of external input is a form of homeostatic plasticity, needed to maintain network stability and variability and depends on intact excitation/inhibition (E/I) balancing mechanisms (64). Nevertheless, aberrant heightened activity and runaway excitation was observed in intracellular recordings, however, only in very few cells. The clustering into cellular and network phenotypes with either very basal or very high activity, especially observed in *week 5* of culturing, could be due to a general heterogeneity in slice viability or potentially even differential changes in transcriptomic profiles influencing homeostatic plasticity and activity, such as the transcription factor family PARbZip (65). A certain degree of neuronal loss takes place during *weeks 4* and *5*, evidenced by the collective drop of RNA expression levels in these culturing periods, as well as parvalbumin-positive neurons and a beginning trend of overall neuronal decline, albeit not significant. An indication of potential degradation in *week 5* was also found in morphological analysis by the significant loss of neuronal complexity. However, the general dendritic arborization of pyramidal neurons in culture closely mimics the *in vivo* maturation process during the first postnatal week (46) and both *in vitro* and *in vivo* results indicate that the final dendritic configuration is established after this time frame. This is highlighted by the fact that coherent morphological changes could not be found in studies investigating mice from P10 onward (45).

Conclusions

In this study, we provided a holistic characterization of the development of the early postnatal mouse neocortex over 5 wk *in vitro*. In summary, the immature cortex underwent a similar maturation as observed *in vivo* in terms of intrinsic and firing properties, network activity, morphology, and RNA expression levels. Cortical oBSCs therefore approach a mature state after ~ 2 wk *in vitro*. Our data indicate that experiments aiming to investigate developmental phenomena of the cortex

are best performed from 0 to 14 days *in vitro*. In contrast, studies requiring an adult configuration of the network, such as simulations of adult brain diseases, will find the cortical network to be most stable and physiologically mature during *weeks 2* and *3* of culturing. Beyond this time frame, rising variability, heterogeneity, excitability, and potential neuronal loss have to be considered, however, cortical cultures aged 4 or 5 wk could potentially serve as models for high-frequency network oscillations.

DATA AVAILABILITY

Data will be made available upon reasonable request.

SUPPLEMENTAL MATERIAL

Supplemental Figs. S1–S7 and Tables S1 and S2: <https://doi.org/10.6084/m9.figshare.26494444>.

ACKNOWLEDGMENTS

Graphical abstract created with BioRender and published with permission.

The authors thank Prof. Dirk Feldmeyer, Dr. Danqing Yang, and Dr. Guanxiao Qi for the provision of electrophysiological equipment and technical assistance.

GRANTS

This work was funded by the Chan Zuckerberg Initiative Collaborative Pairs Project Awards (Phase 1 & Phase 2) and by the German Research Foundation DFG/FNR INTER research unit FOR2715. This work was supported by the “Confocal Microscopy Facility,” a core facility of the Interdisciplinary Center for Clinical Research (IZKF) Aachen within the Faculty of Medicine at RWTH Aachen University.

DISCLOSURES

No conflicts of interest, financial or otherwise, are declared by the authors.

AUTHOR CONTRIBUTIONS

A.B. and H.K. conceived and designed research; A.B., K.S., F.B., O.A.S., and B.G. performed experiments; A.B., M.L.J., F.B., O.A.S., M.J., and K.D.S. analyzed data; A.B., K.M.J.v.L., and H.K. interpreted results of experiments; A.B. prepared figures; A.B. drafted manuscript; A.B., K.S., Y.W., B.K., K.M.J.v.L., and H.K. edited and revised manuscript; A.B., K.S., M.L.J., F.B., O.A.S., B.G., M.J., K.D.S., Y.W., B.K., K.M.J.v.L., and H.K. approved final version of manuscript.

REFERENCES

1. Giandomenico SL, Mierau SB, Gibbons GM, Wenger LMD, Masullo L, Sit T, Sutcliffe M, Boulanger J, Tripodi M, Derivery E, Paulsen O, Lakatos A, Lancaster MA. Cerebral organoids at the air–liquid interface generate diverse nerve tracts with functional output. *Nat Neurosci* 22: 669–679, 2019. doi:10.1038/s41593-019-0350-2.
2. Marchetto MCN, Winner B, Gage FH. Pluripotent stem cells in neurodegenerative and neurodevelopmental diseases. *Hum Mol Genet* 19: R71–R76, 2010. doi:10.1093/hmg/ddq159.
3. Louit A, Galbraith T, Berthod F. In vitro 3D modeling of neurodegenerative diseases. *Bioengineering (Basel)* 10: 93, 2023. doi:10.3390/bioengineering10010093.

4. **Arber C, Lovejoy C, Wray S.** Stem cell models of Alzheimer's disease: progress and challenges. *Alzheimers Res Ther* 9: 42, 2017. doi:10.1186/s13195-017-0268-4.
5. **Bhaduri A, Andrews MG, Mancía Leon W, Jung D, Shin D, Allen D, Jung D, Schmunk G, Haeussler M, Salma J, Pollen AA, Nowakowski TJ, Kriegstein AR.** Cell stress in cortical organoids impairs molecular subtype specification. *Nature* 578: 142–148, 2020. doi:10.1038/s41586-020-1962-0.
6. **Gähwiler BH.** Organotypic cultures of neural tissue. *Trends Neurosci* 11: 484–489, 1988. doi:10.1016/0166-2236(88)90007-0.
7. **Klostermann O, Wahle P.** Patterns of spontaneous activity and morphology of interneuron types in organotypic cortex and thalamus-cortex cultures. *Neuroscience* 92: 1243–1259, 1999. doi:10.1016/s0306-4522(99)00009-3.
8. **Annis CM, O'Dowd DK, Robertson RT.** Activity-dependent regulation of dendritic spine density on cortical pyramidal neurons in organotypic slice cultures. *J Neurobiol* 25: 1483–1493, 1994. doi:10.1002/neu.480251202.
9. **Götz M, Bolz J.** Formation and preservation of cortical layers in slice cultures. *J Neurobiol* 23: 783–802, 1992. doi:10.1002/neu.480230702.
10. **Plenz D, Kitai ST.** Up and down states in striatal medium spiny neurons simultaneously recorded with spontaneous activity in fast-spiking interneurons studied in cortex-striatum-substantia nigra organotypic cultures. *J Neurosci* 18: 266–283, 1997. doi:10.1523/JNEUROSCI.18-01-00266.1998.
11. **McBain CJ, Boden P, Hill RG.** Rat hippocampal slices 'in vitro' display spontaneous epileptiform activity following long-term organotypic culture. *J Neurosci Methods* 27: 35–49, 1989. doi:10.1016/0165-0270(89)90051-4.
12. **Stoppini L, Buchs PA, Muller D.** A simple method for organotypic cultures of nervous tissue. *J Neurosci Methods* 37: 173–182, 1991. doi:10.1016/0165-0270(91)90128-m.
13. **Baratta J, Marienhagen JW, Ha D, Yu J, Robertson RT.** Cholinergic innervation of cerebral cortex in organotypic slice cultures: sustained basal forebrain and transient striatal cholinergic projections. *Neuroscience* 72: 1117–1132, 1996. doi:10.1016/0306-4522(95)00603-6.
14. **Cho S, Wood A, Bowlby MR.** Brain slices as models for neurodegenerative disease and screening platforms to identify novel therapeutics. *Curr Neuropharmacol* 5: 19–33, 2007. doi:10.2174/157015907780077105.
15. **Baker RE, Corner MA, van Pelt J.** Spontaneous neuronal discharge patterns in developing organotypic mega-co-cultures of neonatal rat cerebral cortex. *Brain Res* 1101: 29–35, 2006. doi:10.1016/j.brainres.2006.05.028.
16. **Dong HW, Buonomano DV.** A technique for repeated recordings in cortical organotypic slices. *J Neurosci Methods* 146: 69–75, 2005. doi:10.1016/j.jneumeth.2005.01.017.
17. **Gähwiler BH, Capogna M, Debanne D, McKinney RA, Thompson SM.** Organotypic slice cultures: a technique has come of age. *Trends Neurosci* 20: 471–477, 1997. doi:10.1016/s0166-2236(97)01122-3.
18. **Mewes A, Franke H, Singer D.** Organotypic brain slice cultures of adult transgenic P301S mice—a model for tauopathy studies. *PLoS One* 7: e45017, 2012. doi:10.1371/journal.pone.0045017.
19. **Croft CL, Noble W.** Preparation of organotypic brain slice cultures for the study of Alzheimer's disease. *F1000Res* 7: 592, 2018. doi:10.12688/f1000research.14500.2.
20. **Dong W-Q, Schurr A, Reid KH, Shields CB, West CA.** The rat hippocampal slice preparation as an in vitro model of ischemia. *Stroke* 19: 498–502, 1988. doi:10.1161/01.str.19.4.498.
21. **Pedersen JZ, Bernardi G, Centonze D, Pisani A, Rossi L, Rotilio G, Calabresi P.** Hypoglycemia, hypoxia, and ischemia in a corticostriatal slice preparation: electrophysiological changes and ascorbyl radical formation. *J Cereb Blood Flow Metab* 18: 868–875, 1998. doi:10.1097/00004647-199808000-00006.
22. **Laake JH, Haug F-M, Wieloch T, Ottersen OP.** A simple in vitro model of ischemia based on hippocampal slice cultures and propidium iodide fluorescence. *Brain Res Brain Res Protoc* 4: 173–184, 1999. doi:10.1016/S1385-299X(99)00021-5.
23. **Arias RL, Rene J, Tasse P, Bowlby MR.** Neuroprotective interaction effects of NMDA and AMPA receptor antagonists in an in vitro model of cerebral ischemia. *Brain Res* 816: 299–308, 1999. doi:10.1016/S0006-8993(98)01051-8.
24. **Uesaka N, Hirai S, Maruyama T, Ruthazer ES, Yamamoto N.** Activity dependence of cortical axon branch formation: a morphological and electrophysiological study using organotypic slice cultures. *J Neurosci* 25: 1–9, 2005. doi:10.1523/JNEUROSCI.3855-04.2005.
25. **Bolz JN, Novak N, Götz M, Bonhoeffer T.** Formation of target-specific neuronal projections in organotypic slice cultures from rat visual cortex. *Nature* 346: 359–362, 1990. doi:10.1038/346359a0.
26. **Goel A, Buonomano DV.** Chronic electrical stimulation homeostatically decreases spontaneous activity, but paradoxically increases evoked network activity. *J Neurophysiol* 109: 1824–1836, 2013. doi:10.1152/jn.00612.2012.
27. **Rutherford LC, Dewan A, Lauer HM, Turrigiano GG.** Brain-derived neurotrophic factor mediates the activity-dependent regulation of inhibition in neocortical cultures. *J Neurosci* 17: 4527–4535, 1997. doi:10.1523/JNEUROSCI.17-12-04527.1997.
28. **Raineteau O, Rietschin L, Gradwohl G, Guillemot F, Gähwiler BH.** Neurogenesis in hippocampal slice cultures. *Mol Cell Neurosci* 26: 241–250, 2004. doi:10.1016/j.mcn.2004.01.003.
29. **Muller D, Buchs PA, Stoppini L.** Time course of synaptic development in hippocampal organotypic cultures. *Brain Res Dev Brain Res* 71: 93–100, 1993. doi:10.1016/0165-3806(93)90109-n.
30. **Noraberg J, Poulsen FR, Blaabjerg M, Kristensen BW, Bonde C, Montero M, Meyer M, Gramsbergen JB, Zimmer J.** Organotypic hippocampal slice cultures for studies of brain damage, neuroprotection and neurorepair. *Curr Drug Targets CNS Neurol Disord* 4: 435–452, 2005. doi:10.2174/1568007054546108.
31. **Schurr A, Payne RS, Heine MF, Rigor BM.** Hypoxia, excitotoxicity, and neuroprotection in the hippocampal slice preparation. *J Neurosci Methods* 59: 129–138, 1995. doi:10.1016/0165-0270(94)00203-s.
32. **Buchs P-A, Stoppini L, Muller D.** Structural modifications associated with synaptic development in area CA1 of rat hippocampal organotypic cultures. *Brain Res Dev Brain Res* 71: 81–91, 1993. doi:10.1016/0165-3806(93)90108-m.
33. **Mielke JG, Comas T, Woulfe J, Monette R, Chakravarthy B, Mealing GAR.** Cytoskeletal, synaptic, and nuclear protein changes associated with rat interface organotypic hippocampal slice culture development. *Brain Res Dev Brain Res* 160: 275–286, 2005. doi:10.1016/j.devbrainres.2005.09.009.
34. **Dupont JL, Fourcaudot E, Beekenkamp H, Poulain B, Bossu J-L.** Synaptic organization of the mouse cerebellar cortex in organotypic slice cultures. *Cerebellum* 5: 243–256, 2006. doi:10.1080/14734220600905317.
35. **Birgbauer E, Rao TS, Webb M.** Lysolecithin induces demyelination in vitro in a cerebellar slice culture system. *J Neurosci Res* 78: 157–166, 2004. doi:10.1002/jnr.20248.
36. **Ostergaard K, Finsen B, Zimmer J.** Organotypic slice cultures of the rat striatum: an immunocytochemical, histochemical and in situ hybridization study of somatostatin, neuropeptide Y, nicotinamide adenine dinucleotide phosphate-diaphorase, and enkephalin. *Exp Brain Res* 103: 70–84, 1995. doi:10.1007/BF00241966.
37. **Staal JA, Alexander SR, Liu Y, Dickson TD, Vickers JC.** Characterization of cortical neuronal and glial alterations during culture of organotypic whole brain slices from neonatal and mature mice. *PLoS One* 6: e22040, 2011. doi:10.1371/journal.pone.0022040.
38. **Buonomano DV.** Timing of neural responses in cortical organotypic slices. *Proc Natl Acad Sci USA* 100: 4897–4902, 2003. doi:10.1073/pnas.0736909100.
39. **Johnson HA, Buonomano DV.** Development and plasticity of spontaneous activity and up states in cortical organotypic slices. *J Neurosci* 27: 5915–5925, 2007. doi:10.1523/JNEUROSCI.0447-07.2007.
40. **Caeser M, Bonhoeffer T, Bolz J.** Cellular organization and development of slice cultures from rat visual cortex. *Exp Brain Res* 77: 234–244, 1989. doi:10.1007/BF00274981.
41. **Echevarría D, Albus K.** Activity-dependent development of spontaneous bioelectric activity in organotypic cultures of rat occipital cortex. *Brain Res Dev Brain Res* 123: 151–164, 2000. doi:10.1016/s0165-3806(00)00089-4.
42. **Annis CM, Robertson RT, O'Dowd DK.** Aspects of early postnatal development of cortical neurons that proceed independently of

- normally present extrinsic influences. *J Neurobiol* 24: 1460–1480, 1993. doi:10.1002/neu.480241103.
43. **Oishi Y, Baratta J, Robertson RT, Steward O.** Assessment of factors regulating axon growth between the cortex and spinal cord in organotypic co-cultures: effects of age and neurotrophic factors. *J Neurotrauma* 21: 339–356, 2004. doi:10.1089/089771504322972121.
 44. **Fan J, Stemkowski PL, Gandini MA, Black SA, Zhang Z, Souza IA, Chen L, Zamponi GW.** Reduced hyperpolarization-activated current contributes to enhanced intrinsic excitability in cultured hippocampal neurons from PrP^{0/0} mice. *Front Cell Neurosci* 10: 74, 2016. doi:10.3389/fncel.2016.00074.
 45. **Ciganok-Hückels N, Jehasse K, Kricsfalussy-Hrabár L, Ritter M, Rüländ T, Kampa BM.** Postnatal development of electrophysiological and morphological properties in layer 2/3 and layer 5 pyramidal neurons in the mouse primary visual cortex. *Cereb Cortex* 33: 5875–5884, 2022. doi:10.1093/cercor/bhac467.
 46. **Kroon T, van Hugte E, van Linge L, Mansvelde HD, Meredith RM.** Early postnatal development of pyramidal neurons across layers of the mouse medial prefrontal cortex. *Sci Rep* 9: 5037, 2019. doi:10.1038/s41598-019-41661-9.
 47. **Oswald AMM, Reyes AD.** Maturation of intrinsic and synaptic properties of layer 2/3 pyramidal neurons in mouse auditory cortex. *J Neurophysiol* 99: 2998–3008, 2008. doi:10.1152/jn.01160.2007.
 48. **Feldmeyer D, Radnikow G.** Developmental alterations in the functional properties of excitatory neocortical synapses. *J Physiol* 587: 1889–1896, 2009. doi:10.1113/jphysiol.2009.169458.
 49. **Etherington SJ, Williams SR.** Postnatal development of intrinsic and synaptic properties transforms signaling in the layer 5 excitatory neural network of the visual cortex. *J Neurosci* 31: 9526–9537, 2011. doi:10.1523/JNEUROSCI.0458-11.2011.
 50. **Allen Institute for Brain Science.** Allen Brain Atlas [SCN1A, ID 20265] (Online). <https://developingmouse.brain-map.org/gene/show/20028> [2024 Aug 30].
 51. **Allen Institute for Brain Science.** Allen Developing Mouse Brain Atlas [HCN1, ID 15165] (Online). <https://developingmouse.brain-map.org/gene/show/14941> [2024 Aug 30].
 52. **Liang L, Fazel Darbandi S, Pochareddy S, Gulden FO, Gilson MC, Sheppard BK, Sahagun A, An J-Y, Werling DM, Rubenstein JLR, Sestan N, Bender KJ, Sanders SJ.** Developmental dynamics of voltage-gated sodium channel isoform expression in the human and mouse brain. *Genome Med* 13: 135–14, 2021. doi:10.1186/s13073-021-00949-0.
 53. **Kanyshkova T, Pawlowski M, Meuth P, Dubé C, Bender RA, Brewster AL, Baumann A, Baram TZ, Pape H-C, Budde T.** Postnatal expression pattern of HCN channel isoforms in thalamic neurons: relationship to maturation of thalamocortical oscillations. *J Neurosci* 29: 8847–8857, 2009. doi:10.1523/JNEUROSCI.0689-09.2009.
 54. **Rátkai A, Tárnok K, Aouad HE, Micska B, Schlett K, Szücs A.** Homeostatic plasticity and burst activity are mediated by hyperpolarization-activated cation currents and T-type calcium channels in neuronal cultures. *Sci Rep* 11: 3236, 2021. doi:10.1038/s41598-021-82775-3.
 55. **Sanchez-Vives MV, McCormick DA.** Cellular and network mechanisms of rhythmic recurrent activity in neocortex. *Nat Neurosci* 3: 1027–1034, 2000. doi:10.1038/79848.
 56. **Sakata S, Harris KD.** Laminar structure of spontaneous and sensory-evoked population activity in auditory cortex. *Neuron* 64: 404–418, 2009. doi:10.1016/j.neuron.2009.09.020.
 57. **Bergold PJ, Casaccia-Bonnel P.** Preparation of organotypic hippocampal slice cultures using the membrane filter method. *Methods Mol Biol* 72: 15–22, 1997. doi:10.1385/0-89603-394-5-15.
 58. **Allen Institute for Brain Science.** Allen Developing Mouse Brain Atlas [PVALB, ID 19293] (Online). <https://developingmouse.brain-map.org/gene/show/19056> [2024 Aug 30].
 59. **Sohal VS, Zhang F, Yizhar O, Deisseroth K.** Parvalbumin neurons and gamma rhythms enhance cortical circuit performance. *Nature* 459: 698–702, 2009. doi:10.1038/nature07991.
 60. **Klausberger T, Magill PJ, Márton LF, Roberts JDB, Cobden PM, Buzsáki G, Somogyi P.** Brain-state- and cell-type-specific firing of hippocampal interneurons in vivo. *Nature* 421: 844–848, 2003 [Erratum in *Nature* 441: 902, 2006]. doi:10.1038/nature01374.
 61. **Kalemaki K, Konstantoudaki X, Tivodar S, Sidiropoulou K, Karageorgos D.** Mice with decreased number of interneurons exhibit aberrant spontaneous and oscillatory activity in the cortex. *Front Neural Circuits* 12: 96, 2018. doi:10.3389/fncir.2018.00096.
 62. **Rochefort NL, Garaschuk O, Milos R-I, Narushima M, Marandi N, Pichler B, Kovalchuk Y, Konnerth A.** Sparsification of neuronal activity in the visual cortex at eye-opening. *Proc Natl Acad Sci USA* 106: 15049–15054, 2009. doi:10.1073/pnas.0907660106.
 63. **Brown APY, Cossell L, Margrie TW.** Visual experience regulates the intrinsic excitability of visual cortical neurons to maintain sensory function. *Cell Rep* 27: 685–689.e4, 2019. doi:10.1016/j.celrep.2019.03.073.
 64. **Turrigiano GG, Nelson SB.** Homeostatic plasticity in the developing nervous system. *Nat Rev Neurosci* 5: 97–107, 2004. doi:10.1038/nrn1327.
 65. **Valakh V, Wise D, Zhu XA, Sha M, Fok J, Van Hooser SD, Schectman R, Cepeda I, Kirk R, O'Toole SM, Nelson SB.** A transcriptional constraint mechanism limits the homeostatic response to activity deprivation in mammalian neocortex. *eLife* 12: e74899, 2023. doi:10.7554/eLife.74899.